overwrap with DNA signals (fig. 9*G*). Given that staining of mitochondrial DNA is definitive (fig. 9*F*), the putative plastids seem to contain very low quantities of DNA or may even lack DNA. Our preliminary search of the TIGR genome database suggests that *P. marinus* has genes for mitochondrial DNA and RNA polymerases, elongation factors, and ribosomal proteins but seemingly lacks those for plastid counterparts (data not shown). There are no examples in the literature of DNA-lacking plastids; however, we know of many independent reports that show modified or degenerated mitochondria that lack DNA (Hackstein et al. 2006). It is thus worth considering the possibility of DNA-lacking plastids in *P. marinus*, although this remains to be confirmed experimentally.

We have shown the presence of secondary plastids in *P. marinus* by immunofluorescent microscopy; however, no corresponding structure has been found in EM specimens sampled from the same culture (Kuroiwa H, unpublished data). Upon conducting a literature review, we found that 3 candidate ultrastructures have been observed in allied organisms. One is a "coiled membrane system" near the mitochondria that was found in the oldest observations of *P. marinus* zoosporulation (Perkins and Menzel 1967). Although this structure has been considered a morphological variant of the mitochondria, it could also be interpreted as a multimembrane-bounded plastid resembling the apicoplast of the malarial parasite *Plasmodium falciparum* (Hopkins et al. 1999). Another candidate structure is the "enigmatic body" found in a related organism, *Rastrimonas subtilis* (Brugerolle 2002, 2003), which is limited by 2 or more membranes and is akin to the apicoplast of *Toxoplasma gondii* in spherical appearance and juxtanuclear localization (Matsuzaki et al. 2001; Köhler 2005); however, the assumed relationship between *R. subtilis* and *Perkinsus* spp. is based only on morphology and is currently unsupported by molecular information. Finally, a putative plastid bounded by 4 membranes was recently reported in *P. olseni* (=*P. atlanticus*) (Teles-Grilo et al. 2007). If this is the plastid to which the MEP pathway enzymes target, connection between the TP with a transmembrane helix and a plastid bounded by 3 membranes should be reconsidered. It is interesting that all 3 candidate structures have been observed in the respective organisms' flagellated stage and that no relevant structures have been reported at the EM level from nonflagellated cultures. Our results indicate that the nonflagellated cultures contain plastids (fig. 9*B*). It is possible that the plastid is in a degenerated form and is therefore overlooked in the nonflagellated stages at the EM level and develops during the course of differentiation into the flagellated stages. Note that ultrastructure alone (e.g., number of membranes) is inadequate to identify plastids (Köhler 2006); immunological labeling of the ultrastructure is required for confirmation, for which our affinity-purified antibody to ispC would be useful.

That the putative *P. marinus* plastid and the peridinine plastids share a common origin was suggested by the phylogenetic affinity between some MEP pathway genes and those of the peridinine dinoflagellates and the predicted features of the *P. marinus* TPs. The *P. marinus* TPs predict that the putative plastid is bounded by 3 membranes because TP with transmembrane helix seems to correspond to plastids with 3 bounding membranes, such as those found in dinoflagellates and euglenoids (Patron et al. 2005). Given that *Perkinsus* spp. are located basally to dinoflagellates (Cavalier-Smith and Chao 2004; Leander and Keeling 2004), it is reasonable to suppose that a common ancestor harbored a plastid that diverged to form the *P. marinus* and peridinine plastids. *Perkinsus marinus* has TPs that are reminiscent of those found in peridinine dinoflagellates (fig. 1), although unusual TPs have been found in dinoflagellates containing haptophyte-derived plastids (Patron et al. 2006); thus, the result supports the hypothesis that haptophyte-derived plastids are a derived feature (Yoon et al. 2005). Study of the MEP pathway genes in other nonphotosynthetic taxa of Dinozoa, such as *Oxyrrhis*, *Syndinium*, and *Noctiluca*, may reveal the presence of cryptic plastids. On the other hand, the *Perkinsus* MEP pathway genes failed to show a relationship with apicomplexan orthologs (data not shown) possibly because the apicomplexan OTUs were a strong source of a long-branch attraction artifact. The relationship between the putative plastid of *P. marinus* and the apicoplast is thus still open question. Because the nonphotosynthetic free-living flagellates, *Colpodella* spp., are phylogenetically basal to the apicomplexans (Kuvardina et al. 2002; Cavalier-Smith and Chao 2004; Skovgaard et al. 2005), investigating whether *Colpodella* contains plastids would be interesting. The putative plastid in *P. marinus* will be a key to verifying the chromalveolate hypothesis and will partially rebut its critics (Bodył 2005).

Implications for Plastid Evolution

Our phylogenetic analyses showed that the MEP pathway of PBEs has an apparently mosaic origin in Cyanobacteria, Proteobacteria, and Chlamydia (table 1). Although an earlier study with limited sampling gave similar results for 5 genes (dxs to ispF) (Lange et al. 2000), the present results reinforce the evolutionary origins by using a wide range of bacteria. We also showed that the mosaic pattern was essentially the same among PBEs, including *P. marinus*, as is often the case with other plastid-related mosaic pathways, such as the Calvin cycle, heme biosynthesis, and the shikimate pathway (Matsuzaki et al. 2004; Obornik and Green 2005; Richards et al. 2006). Thus, we assume that the mosaic pattern was established before radiation of a wide variety of plastids, again supporting a single origin for plastids (Bhattacharya et al. 2004; Matsuzaki et al. 2004). It is natural that the cyanobacterial genes would be introduced during the primary endosymbiotic event, but the contribution of chlamydial genes seems rather peculiar. The apparent affinity could be interpreted as an artifact of interbacterial gene replacement (Lange et al. 2000; Rujan and Martin 2001); however, we consider that the observed mosaic pattern reflects an actual contribution by Chlamydia, because Chlamydia-related higher plant genes are biased toward plastid functions (Brinkman et al. 2002), and the bias is difficult to explain without assuming a connection between Chlamydia and plastids.

The ispG alignment (supplementary fig. S2, Supplementary Material online) and phylogenetic tree (fig. 6) show that the origin of the red algal orthologs clearly differed from that of orthologs from other PBEs. This seems

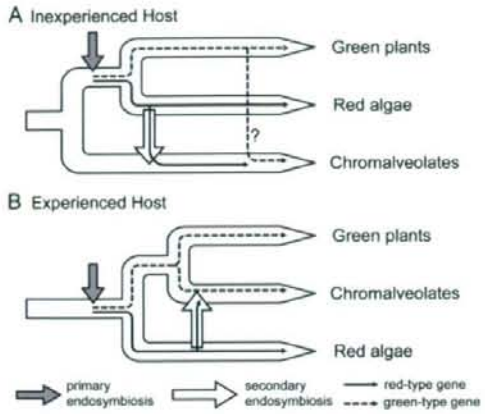

FIG. 10.—Explanation of the phylogenetic affinity to green plants in the cyanobacterial genes from chromalveolates, in 2 alternative phylogenetic trees of the host eukaryotes. (*A*) The inexperienced host model. If the ancestral chromalveolate host was inexperienced with primary plastids, red-type genes (solid arrows) must have been introduced and used in the chromalveolates at the secondary endosymbiotic event (unfilled arrow). Then, the green-type genes (broken arrows) may have been introduced via an unknown lateral gene transfer (LGT) event (indicated by "?") and replaced the red-type genes. (*B*) The experienced host model. Assuming that the ancestral host organism was experienced with primary plastids, 2 options exist for the secondary endosymbiotic event: retaining the green-type genes inherited from the ancestor or accepting the red-type genes transferred from the symbiont. In this case, the discrepancy can be explained without any further LGT event.

unusual, but other genes also show a similar difference between red algae and other PBEs, for example, enoyl acyl carrier protein reductase (Matsuzaki M, unpublished data) and plastid ferrochelatase (Oborník and Green 2005). This discrepancy in the phylogenetic positions of genes in red algae and the chromalveolates can be explained by the evolutionary histories of the symbiotic hosts (fig. 10). Two competing inferences exist for PBE phylogeny: the chromalveolates are independent of primary PBEs and are inexperienced with primary plastids (Rodríguez-Ezpeleta et al. 2005) (fig. 10*A*) and the chromalveolates originate from an in-group of primary PBEs and are experienced with primary plastids (Nozaki et al. 2003, 2007) (fig. 10*B*). Because it is widely accepted that the plastid progenitor in the chromalveolates is a kind of, or belongs to a sister group of, ancestral red algae (Fast et al. 2001; Yoon et al. 2002, 2005), the former topology predicts that red algae and the chromalveolates contain genes of the same cyanobacterial origin and requires extra loss, gain, or transfer events to explain the observed differences (fig. 10*A* shows a transfer event from the green plant lineage, which is the simplest). For the latter topology, the chromalveolates have 2 possible sources for plastid genes, the host ancestor and the symbiont. In this scenario, genes related to those of green plants can be inherited as constituents of the host genome and can be retained and used after the secondary endosymbiotic event. We prefer the latter model (fig. 10*B*) because it does not require additional transfer events other than the 2 widely accepted endosymbiotic events. In addition, this scenario can explain the frequently observed incoherence of the phylogenetic affinity of diatom genes, for example, the MEP pathway (figs. 2–7), the shikimate pathway (Richards et al. 2006), and the heme biosynthesis pathway (Oborník and Green 2005), in which the diatom ortholog for each gene has phylogenetic affinities to either green plants or red algae. Genes with an affinity to green plants and red algae could be derived from the host eukaryote and the plastid progenitor at the secondary symbiotic event, respectively. Furthermore, this scenario implies that the host eukaryote of the secondary endosymbiotic event that forms the chromalveolate ancestor must have retained the primary plastid originating from the ancient primary endosymbiosis because the MEP pathway seems to be specific to PBEs; then, it was replaced with the secondary plastid obtained from the engulfed red alga.

Conclusion

The existence of the plastid and its affinity to those of dinoflagellates, as suggested in the present study, greatly changes our view of *P. marinus*. It was first described as a pathogenic protist, then subsequently reclassified as a fungal or sporozoan species, and has recently been treated as an alveolate flagellate (Villalba et al. 2004; Adl et al. 2005); however, *P. marinus* is a cryptic alga in terms of plastid existence. Our identification of a *Perkinsus* spp. plastid will make this algal organism key in discussions of plastid evolution. Furthermore, just as discovery of the apicoplast has revolutionized malaria chemotherapy, the algal nature of *Perkinsus* spp. may permit novel approaches for controlling perkinsosis in fisheries.

Supplementary Material

Supplementary tables S1–S3 and figures S1–S3 are available at *Molecular Biology and Evolution* online (http://www.mbe.oxfordjournals.org/).

Acknowledgments

Preliminary sequence data for *P. marinus* were obtained from The Institute for Genomic Research via their Web site at http://www.tigr.org/. Sequencing of the *P. marinus* genome was accomplished with support from the US National Science Foundation. The genome sequence data for *Galdieria sulphuraria* were obtained from the Michigan State University Galdieria Database (http://genomics.msu.edu/galdieria/). The genome sequence data for *Chlamydomonas reinhardtii*, *Ostreococcus lucimarinus*, *Phaeodactylum tricornutum*, and *Thalassiosira pseudonana* were obtained from the US Department of Energy Joint Genome Institute (http://www.jgi.doe.gov/) and are provided for use in this publication only. The authors thank Dr Shin-ichiro Maruyama and Dr Takashi Nakada (the University of Tokyo) for helpful discussions and comments on figure presentation and Dr Shigeharu Sato (National Institute for Medical Research, UK) for providing valuable information on related topics. This study was supported by Grants-in-Aid

for Creative Scientific Research (16GS0304 to H.N. and 18GS0314 to K.K.), for Scientific Research (17370087 to H.N. and 18073004 for K.K.), and for the Japan Society for the Promotion of Science (JSPS) Fellows (17-10695 to M.M.) from the JSPS and the Ministry of Education, Culture, Sports, Science, and Technology (MEXT); by a matching fund subsidy for "Academic Frontier" Projects (to T.K.) from MEXT; and by the Program for the Promotion of Basic Research Activities for Innovative Biosciences (to T.K.). M.M. is a Research Fellow of the JSPS.

Literature Cited

Adl SM, Simpson AGB, Farmer MA, et al. (28 co-authors). 2005. The new higher level classification of eukaryotes with emphasis on the taxonomy of protists. J Eukaryot Microbiol. 52:399–451.

Armougom F, Moretti S, Poirot O, Audic S, Dumas P, Schaeli B, Keduas V, Notredame C. 2006. Expresso: automatic incorporation of structural information in multiple sequence alignments using 3D-Coffee. Nucleic Acids Res. 34:W604–W608.

Bendtsen JD, Nielsen H, von Heijne G, Brunak S. 2004. Improved prediction of signal peptides: signalP 3.0. J Mol Biol. 340:783–795.

Bhattacharya D, Yoon HS, Hackett JD. 2004. Photosynthetic eukaryotes unite: endosymbiosis connects the dots. Bioessays. 26:50–60.

Bodył A. 2005. Do plastid-related characters support the chromalveolate hypothesis? J Phycol. 41:712–719.

Brinkman FSL, Blanchard JL, Cherkasov A, et al. (14 co-authors). 2002. Evidence that plant-like genes in Chlamydia species reflect an ancestral relationship between Chlamydiaceae, cyanobacteria, and the chloroplast. Genome Res. 12:1159–1167.

Brugerolle G. 2002. *Cryptophagus subtilis*: a new parasite of cryptophytes affiliated with the Perkinsozoa lineage. Eur J Protistol. 37:379–390.

Brugerolle G. 2003. Apicomplexan parasite *Cryptophagus* renamed *Rastrimonas* gen. nov. Eur J Protistol. 39:101.

Cavalier-Smith T. 1999. Principles of protein and lipid targeting in secondary symbiogenesis: euglenoid, dinoflagellate, and sporozoan plastid origins and the eukaryote family tree. J Eukaryot Microbiol. 46:347–366.

Cavalier-Smith T, Chao EE. 2004. Protalveolate phylogeny and systematics and the origins of Sporozoa and dinoflagellates (phylum Myzozoa nom. nov.). Eur J Protistol. 40:185–212.

Derelle E, Ferraz C, Rombauts S, et al. (26 co-authors). 2006. Genome analysis of the smallest free-living eukaryote *Ostreococcus tauri* unveils many unique features. Proc Natl Acad Sci USA. 103:11647–11652.

Edgar RC. 2004. MUSCLE: multiple sequence alignment with high accuracy and high throughput. Nucleic Acids Res. 32:1792–1797.

Emanuelsson O, Nielsen H, Brunak S, von Heijne G. 2000. Predicting subcellular localization of proteins based on their N-terminal amino acid sequence. J Mol Biol. 300:1005–1016.

Fast NM, Kissinger JC, Roos DS, Keeling PJ. 2001. Nuclear-encoded, plastid-targeted genes suggest a single common origin for apicomplexan and dinoflagellate plastids. Mol Biol Evol. 18:418–426.

Gardner MJ, Bishop R, Shah T, et al. (44 co-authors). 2005. Genome sequence of *Theileria parva*, a bovine pathogen that transforms lymphocytes. Science. 309:134–137.

Gardner MJ, Hall N, Fung E, et al. (45 co-authors). 2002. Genome sequence of the human malaria parasite *Plasmodium falciparum*. Nature. 419:498–511.

Goto N, Nakao MC, Kawashima S. 2003. BioRuby: open-source bioinformatics library. Genome Inform. 14:629–630.

Guindon S, Gascuel O. 2003. A simple, fast, and accurate algorithm to estimate large phylogenies by maximum likelihood. Syst Biol. 52:696–704.

Hackstein JHP, Tjaden J, Huynen M. 2006. Mitochondria, hydrogenosomes and mitosomes: products of evolutionary tinkering! Curr Genet. 50:225–245.

Hirokawa T, Boon-Chieng S, Mitaku S. 1998. SOSUI: classification and secondary structure prediction system for membrane proteins. Bioinformatics. 14:378–379.

Hopkins J, Fowler R, Krishna S, Wilson I, Mitchell G, Bannister L. 1999. The plastid in *Plasmodium falciparum* asexual blood stages: a three-dimensional ultrastructural analysis. Protist. 150:283–295.

Köhler S. 2005. Multi-membrane-bound structures of Apicomplexa: I. the architecture of the *Toxoplasma gondii* apicoplast. Parasitol Res. 96:258–272.

Köhler S. 2006. Multi-membrane-bound structures of Apicomplexa: II. the ovoid mitochondrial cytoplasmic (OMC) complex of *Toxoplasma gondii* tachyzoites. Parasitol Res. 98: 355–369.

Kuvardina ON, Leander BS, Aleshin VV, Myl'nikov AP, Keeling PJ, Simdyanov TG. 2002. The phylogeny of colpodellids (Alveolata) using small subunit rRNA gene sequences suggests they are the free-living sister group to apicomplexans. J Eukaryot Microbiol. 49:498–504.

Lange BM, Rujan T, Martin W, Croteau R. 2000. Isoprenoid biosynthesis: the evolution of two ancient and distinct pathways across genomes. Proc Natl Acad Sci USA. 97:13172–13177.

Leander BS, Keeling PJ. 2004. Early evolutionary history of dinoflagellates and apicomplexans (Alveolata) as inferred from hsp90 and actin phylogenies. J Phycol. 40:341–350.

Matsuzaki M, Kikuchi T, Kita K, Kojima S, Kuroiwa T. 2001. Large amounts of apicoplast nucleoid DNA and its segregation in *Toxoplasma gondii*. Protoplasma. 218:180–191.

Matsuzaki M, Misumi O, Shin-i T, et al. (42 co-authors). 2004. Genome sequence of the ultrasmall unicellular red alga *Cyanidioschyzon merolae* 10D. Nature. 428:653–657.

Nielsen H, Engelbrecht J, Brunak S, von Heijne G. 1997. Identification of prokaryotic and eukaryotic signal peptides and prediction of their cleavage sites. Protein Eng. 10:1–6.

Nielsen H, Krogh A. 1998. Prediction of signal peptides and signal anchors by a hidden Markov model. Proc Int Conf Intell Syst Mol Biol. 6:122–130.

Not F, Valentin K, Romari K, Lovejoy C, Massana R, Töbe K, Vaulot D, Medlin LK. 2007. Picobiliphytes: a marine picoplanktonic algal group with unknown affinities to other eukaryotes. Science. 315:253–255.

Nozaki H, Iseki M, Hasegawa M, Misawa K, Nakada T, Sasaki N, Watanabe M. 2007. Phylogeny of primary photosynthetic eukaryotes as deduced from slowly evolving nuclear genes. Mol Biol Evol. 24:1592–1595.

Nozaki H, Matsuzaki M, Takahara M, Misumi O, Kuroiwa H, Hasegawa M, Shin-i T, Kohara Y, Ogasawara N, Kuroiwa T. 2003. The phylogenetic position of red algae revealed by multiple nuclear genes from mitochondria-containing eukaryotes and an alternative hypothesis on the origin of plastids. J Mol Evol. 56:485–497.

Obornik M, Green BR. 2005. Mosaic origin of the heme biosynthesis pathway in photosynthetic eukaryotes. Mol Biol Evol. 22:2343–2353.

Patron NJ, Waller RF, Archibald JM, Keeling PJ. 2005. Complex protein targeting to dinoflagellate plastids. J Mol Biol. 348: 1015–1024.

Patron NJ, Waller RF, Keeling PJ. 2006. A tertiary plastid uses genes from two endosymbionts. J Mol Biol. 357:1373–1382.

Perkins FO. 1976. Zoospores of the oyster pathogen, *Dermocystidium marinum*. I. Fine structure of the conoid and other sporozoan-like organelles. J Parasitol. 62:959–974.

Perkins FO. 1996. The structure of *Perkinsus marinus* (Mackin, Owen and Collier, 1950) Levine, 1978 with comments on taxonomy and phylogeny of Perkinsus spp. J Shellfish Res. 15:67–87.

Perkins FO, Menzel RW. 1967. Ultrastructure of sporulation in the oyster pathogen *Dermocystidium marinum*. J Invertebr Pathol. 9:205–229.

Richards TA, Dacks JB, Campbell SA, Blanchard JL, Foster PG, McLeod R, Roberts CW. 2006. Evolutionary origins of the eukaryotic shikimate pathway: gene fusions, horizontal gene transfer, and endosymbiotic replacements. Eukaryot Cell. 5:1517–1531.

Rodríguez-Concepción M. 2004. The MEP pathway: a new target for the development of herbicides, antibiotics and antimalarial drugs. Curr Pharm Des. 10:2391–2400.

Rodríguez-Ezpeleta N, Brinkmann H, Burey SC, Roure B, Burger G, Löffelhardt W, Bohnert HJ, Philippe H, Lang BF. 2005. Monophyly of primary photosynthetic eukaryotes: green plants, red algae, and glaucophytes. Curr Biol. 15:1325–1330.

Rujan T, Martin W. 2001. How many genes in Arabidopsis come from cyanobacteria? An estimate from 386 protein phylogenies. Trends Genet. 17:113–120.

Schott EJ, Vasta GR. 2003. The *PmSOD1* gene of the protistan parasite *Perkinsus marinus* complements the *sod2Δ* mutant of *Saccharomyces cerevisiae*, and directs an iron superoxide dismutase to mitochondria. Mol Biochem Parasitol. 126:81–92.

Skovgaard A, Massana R, Balagué V, Saiz E. 2005. Phylogenetic position of the copepod-infesting parasite *Syndinium turbo* (Dinoflagellata, Syndinea). Protist. 156:413–423.

Stelter K, El-Sayed NM, Seeber F. 2007. The expression of a plant-type ferredoxin redox system provides molecular evidence for a plastid in the early dinoflagellate *Perkinsus marinus*. Protist. 158:119–130.

Sunila I, Hamilton RM, Dungan CF. 2001. Ultrastructural characteristics of the in vitro cell cycle of the protozoan pathogen of oysters, *Perkinsus marinus*. J Eukaryot Microbiol. 48:348–361.

Teles-Grilo ML, Tato-Costa J, Duarte SM, Maia A, Casal G, Azevedo C. 2007. Is there a plastid in *Perkinsus atlanticus* (Phylum Perkinsozoa)? Eur J Protistol. 43:163–167.

Thompson JD, Gibson TJ, Plewniak F, Jeanmougin F, Higgins DG. 1997. The CLUSTAL_X windows interface: flexible strategies for multiple sequence alignment aided by quality analysis tools. Nucleic Acids Res. 25:4876–4882.

van Dooren GG, Schwartzbach SD, Osafune T, McFadden GI. 2001. Translocation of proteins across the multiple membranes of complex plastids. Biochim Biophys Acta. 1541: 34–53.

Villalba A, Reece KS, Ordás MC, Casas SM, Figueras A. 2004. Perkinsosis in molluscs: a review. Aquat Living Resour. 17:411–432.

Whelan S, Goldman N. 2001. A general empirical model of protein evolution derived from multiple protein families using a maximum-likelihood approach. Mol Biol Evol. 18:691–699.

Wilson RJM. 2005. Parasite plastids: approaching the endgame. Biol Rev Camb Philos Soc. 80:129–153.

Wright AC, Ahmed H, Gauthier JD, Silva AM, Vasta GR. 2002. cDNA cloning and characterization of two iron superoxide dismutases from the oyster parasite *Perkinsus marinus*. Mol Biochem Parasitol. 123:73–77.

Yoon HS, Hackett JD, Pinto G, Bhattacharya D. 2002. The single, ancient origin of chromist plastids. Proc Natl Acad Sci USA. 99:15507–15512.

Yoon HS, Hackett JD, Van Dolah FM, Nosenko T, Lidie KL, Bhattacharya D. 2005. Tertiary endosymbiosis driven genome evolution in dinoflagellate algae. Mol Biol Evol. 22: 1299–1308.

Takashi Gojobori, Associate Editor

Accepted March 14, 2008

Please cite this article in press as: Hirai et al., Male Fertility of Malaria Parasites Is Determined by GCS1, a Plant-Type Reproduction Factor, Current Biology (2008), doi:10.1016/j.cub.2008.03.045

Current Biology 18, 1–7, April 22, 2008 ©2008 Elsevier Ltd All rights reserved DOI 10.1016/j.cub.2008.03.045

Report

Male Fertility of Malaria Parasites Is Determined by GCS1, a Plant-Type Reproduction Factor

Makoto Hirai,[1,8,*] Meiji Arai,[2,8] Toshiyuki Mori,[3,8] Shin-ya Miyagishima,[3] Satoru Kawai,[4] Kiyoshi Kita,[5] Tsuneyoshi Kuroiwa,[6] Olle Terenius,[7] and Hiroyuki Matsuoka[1]

[1]Division of Medical Zoology
Department of Infection and Immunity
Jichi Medical University School of Medicine
Shimotsuke City, Tochigi 329-0498
Japan

[2]Department of Immunology and Parasitology
University of Occupational and Environmental Health, Japan
Kitakyusyu, Fukuoka 807-8555
Japan

[3]Miyagishima Initiative Research Unit
RIKEN Frontier Research System
Wako, Saitama 351-0198
Japan

[4]Department of Tropical Medicine and Parasitology
Dokkyo University School of Medicine
Mibu, Tochigi 321-0293
Japan

[5]Department of Biomedical Chemistry
Graduate School of Medicine
The University of Tokyo
Hongo, Tokyo 113-0033
Japan

[6]Research Information Center for Extremophile
Rikkyo (St. Paul's) University
Toshimaku, Tokyo 171-8501
Japan

[7]Department of Molecular Biology and Biochemistry
University of California
3205 McGaugh Hall
Irvine, California 92697

Summary

Malaria, which is caused by *Plasmodium* parasites, is transmitted by anopheline mosquitoes. When gametocytes, the precursor cells of *Plasmodium* gametes, are transferred to a mosquito, they fertilize and proliferate, which render the mosquito infectious to the next vertebrate host [1]. Although the fertilization of malaria parasites has been considered as a rational target for transmission-blocking vaccines [2], the underlying mechanism is poorly understood. Here, we show that the rodent malaria parasite gene *Plasmodium berghei* GENERATIVE CELL SPECIFIC 1 (PbGCS1) plays a central role in its gametic interaction. *PbGCS1* knockout parasites show male sterility, resulting in unsuccessful fertilization. Because such a male-specific function of GCS1 has been observed in angiosperms [3, 4], this indicates, for the first time, that parasite sexual reproduction is controlled by a machinery common to flowering plants. Our present findings provide a new viewpoint for understanding the parasitic fertilization system and important clues for novel strategies to attack life-threatening parasites.

Results and Discussion

GCS1 Is Highly Conserved in *Plasmodium* and Other Organisms

Our previous study revealed that angiosperm GCS1 has an exclusive function in male fertility and that putative *GCS1* genes are widely conserved in various organisms including the human malaria *P. falciparum*, (AAN35337) [3]. To investigate whether malaria GCS1 has a role in parasite fertilization similar to that of angiosperm GCS1, we searched for homologous sequences in the rodent malaria parasite *P. berghei* because this parasite is amenable to gene targeting [5] and its fertilization can be easily evaluated in vitro and in vivo [6]. As a result, the sequence PB000710.01.0 (PlasmoDB) was detected as only one putative *GCS1* candidate (*PbGCS1*). The full-length *PbGCS1* cDNA from the gamete stage was cloned and found to have an N-terminal signal sequence and a C-terminal transmembrane domain, typical of GCS1s (Figure 1A). Further database analysis indicated that *GCS1*s are present in other parasites (*Cryptosporidium parvum*, *Leishmania major*, and *Trypanosoma cruzi*) besides malaria parasites (*P. yoelii* and *P. vivax*) as a single-copy gene. In addition, genomes of amoeba (*Dictyostelium discoideum* and *Physarum polycephalum*) and some animal species (*Monosiga brevicollis*, *Hydra magnipapillata*, and *Nematostella vectensis*) also possess a *GCS1*-like gene. The widespread distribution of *GCS1*-like genes in major eukaryotic kingdoms suggests that the origin of *GCS1*-like genes is close to the origin of eukaryotes [3]. (Figures 1B and 1C).

PbGCS1 Is Expressed in Male Gametocytes and Gametes

To investigate PbGCS1 expression, we generated a transgenic *P. berghei* expressing PbGCS1 fused with Azami Green Fluorescent Protein (AGFP) (PbGCS1::AGFP) under the endogenous *PbGCS1* promoter (Figures 2A and 2B). A subpopulation of erythrocytes infected with *PbGCS1::AGFP* parasites showed fluorescent signals (Figures 2C and 2D). The parasitized blood was incubated in gametogenesis-inducing medium [7] to observe gametocytes and gametes. The exflagellation of PbGCS1::AGFP-expressing cells (>70%) occurred 15 min after induction, indicating that PbGCS1 is expressed in male gametocytes and gametes. Due to the swift motility of male flagella, it was difficult to observe fluorescence in them. To facilitate observation of flagella, the *PbGCS1::AGFP* parasites were immunostained with anti-AGFP antibody. As a result, AGFP signals were detected in both exflagellating male gametes and flagella (Figures 2E–2G). The expression of PbGCS1 also was investigated in female gametes. The *PbGCS1::AGFP* transformants were incubated in gametogenesis-inducing medium under the condition in which their fertilization is inhibited by male inactivation with aphidicolin treatment, whereas females transform into functional gametes [6]. To discriminate the female gametes from AGFP-expressing cells, the transformants

*Correspondence: mhirai@ms.jichi.ac.jp
[8]These authors contributed equally to this work.

Please cite this article in press as: Hirai et al., Male Fertility of Malaria Parasites Is Determined by GCS1, a Plant-Type Reproduction Factor, Current Biology (2008), doi:10.1016/j.cub.2008.03.045

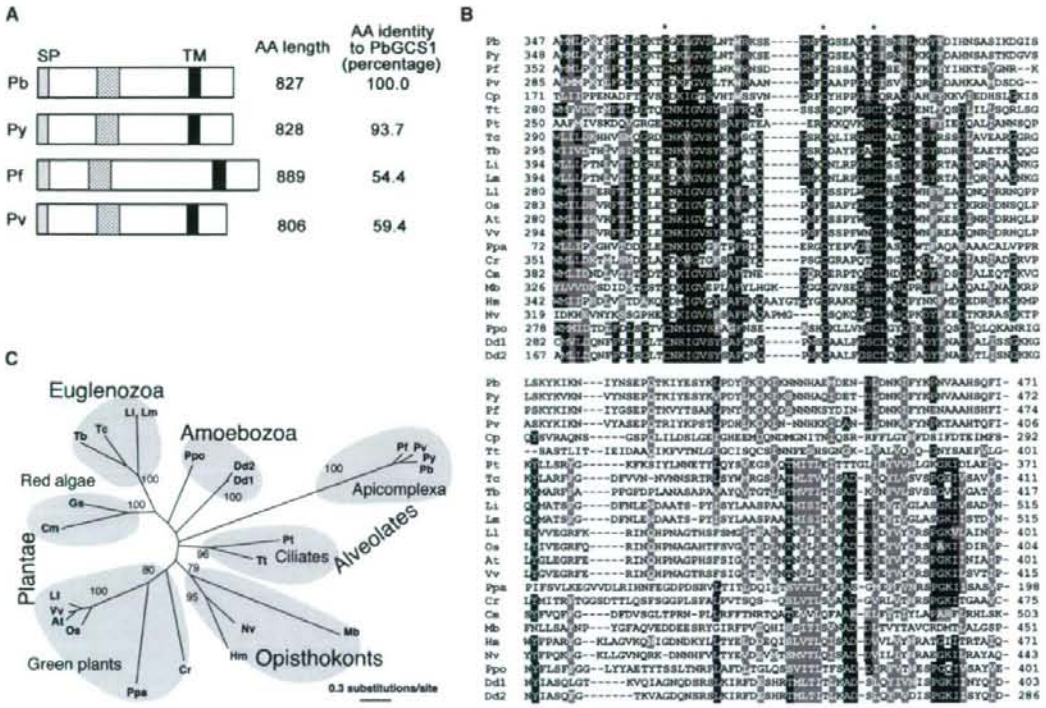

Figure 1. Primary Structure of PbGCS1

(A) GCS1 homologs in *P. berghei* (Pb), *P. yoelii* (Py), *P. falciparum* (Pf), and *P. vivax* (Pv). Abbreviations: SP, putative signal peptide; and TM, transmembrane region. Previously identified conserved regions [3] are indicated by hatched boxes, and alignment is shown in (B).

(B) Comparison of the amino acid sequences conserved among the GCS1 homologs. Identical and conserved residues are shaded black and gray, respectively. Notably, three cysteine residues are completely conserved among all homologs (asterisks).

(C) A maximum-likelihood tree of GCS1 homologs. The tree includes sequences of kinetoplastids (Euglenozoa; Tb, Tc), Amoebozoa (Ppo, Dd), ciliates (Alveolata; Pt, Tt), Apicomplexa (Alveolata; Pt, Pv, Py, Pb), animals (Opisthokonta; Hm, Nv) Choanozoa (Opisthokonta; Mb), plants (green plants in Plantae; Li, Vv, At, Os, Ppa), a green alga (green plants in Plantae; Cr), and red algae (Plantae; Cm, Gs). A deduced GsGCS1 sequence was obtained from the *Galdieria sulphuraria* genome project (http://genomics.msu.edu/cgi-bin/galdieria/blast.cgi). Numbers at the nodes are local bootstrap values calculated by using PhyML analyses. Bootstrap values >75% are shown at the selected nodes. Branch lengths are proportional to the number of amino acid substitutions, which are indicated by the scale bar below the tree. Abbreviations: At, *Arabidopsis thaliana*; Cm, *Cyanidioschyzon merolae*; Cp, *Cryptosporidium parvum*; Cr, *Chlamydomonas reinhardtii*; Dd, *Dictyostelium discoideum*; Gs, *Galdieria sulphuraria*; Hm, *Hydra magnipapillata*; Li, *Leishmania infantum*; Li, *Lilium longiflorum*; Lm, *Leishmania major*; Mb, *Monosiga brevicollis*; Nv, *Nematostella vectensis*; Os, *Oryza stiva*; Ppa, *Physcomitrella patens*; Ppo, *Physarum polycephalum*; Tb, *Trypanosoma brucei*; Tc, *Trypanosoma cruzi*; Tt, *Tetrahymena thermophila*; Pt, *Paramecium tetraurelia*; and Vv, *Vitis vinifera*.

were immunostained with AGFP antibody and a monoclonal antibody against Pbs21, which is a marker protein for female gametes, zygotes, and ookinetes [8]. By observing more than 150 female gametes obtained from at least three independent experiments, we confirmed that all Pbs21-positive female gametes were AGFP-negative and vice versa. This suggests that PbGCS1 is not expressed in female gametes (Figures 2H–2K). These observations indicate that the *GCS1* gene is likely to be exclusively expressed in the male gametocytes and gametes. Next, we investigated the PbGCS1 expression in ookinetes, which is a postfertilization stage. To avoid any adverse effects caused by the PbGCS1 modifications, a transgenic *P. berghei* expressing AGFP under the *PbGCS1* promoter was generated (*PbGCS1prom::AGFP*) (Figures S1A and S1B available online). The transformants underwent normal asexual and sexual stage development in vivo and showed male specific AGFP expression (Figure S1C), whereas no fluorescent signal was detected in ookinetes (Figure S1D). Taken together, *PbGCS1* is expressed only in male gametocytes and gametes, and its expression level is rapidly decreased after fertilization.

PbGCS1 Is Essential for Parasite Fertilization

To address the PbGCS1 functions, we generated *PbGCS1*(−) *P. berghei* (Figure 3A) and performed phenotypic analyses. Three independent clones (1–3, 2–5, and 3–6) were established, and the correct targeting event in each clone was confirmed by diagnostic PCR and Southern blot analysis (Figures 3B and 3C). The morphology of *PbGCS1*(−) gametocytes was indistinguishable from normal parasites (Figure 3D). *PbGCS1*(−) parasites underwent normal development of asexual blood stages and gametocyte formation in mice (further described in Table S1).

Please cite this article in press as: Hirai et al., Male Fertility of Malaria Parasites Is Determined by GCS1, a Plant-Type Reproduction Factor, Current Biology (2008), doi:10.1016/j.cub.2008.03.045

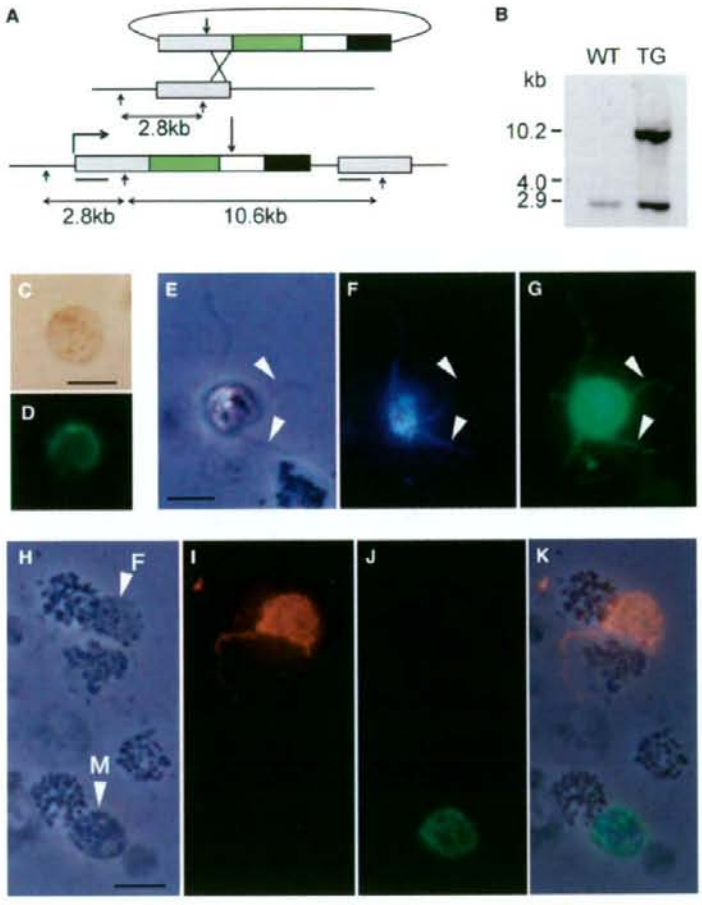

Figure 2. Generation and Characterization of the Transgenic Parasite Line *PbGCS1::AGFP*

(A) Schematic representation of AGFP tagging of the *PbGCS1* locus using a plasmid that integrated through single crossover homologous recombination. The boxes indicate *PbGCS1* gene (gray), *AGFP* (green), 3′ UTR of *PbGCS1* gene (white) and *TgDHFR/ts* selectable marker (black). "E" indicates EcoRI digestion site. For the transfection experiment, the plasmid was cut with the EcoRI site in the *PbGCS1* gene. Bars represent the position of the probe used in Southern blot analysis.

(B) Southern blot genotyping confirmed gene integration. Hybridization of the probe with EcoRI-digested genomic DNA yielded a 2.8 kb WT and 2.8 and 10.6 kb transgenic (TG) bands.

(C) Live PbGCS1::AGFP-expressing cells.

(D) The fluorescent signal of the same cell in (C).

(E–G) An exflagellating male was immunostained with anti-AGFP antibody. (E) Bright field. (F) Nuclear staining with DAPI. (G) PbGCS1::AGFP expression. Arrows indicate flagella being released.

(H–K) The gametes from the transgenic line were double stained with anti-Pbs21 (I) and anti-AGFP (J). "F" and "M" in (H) indicate female and male gamete, respectively. Bars represent 5 μm.

We investigated the infectivity of *PbGCS1*(−) parasites for mosquitoes and subsequent transmission to mice. As control knockout parasites possess wild-type *PbGCS1*, we generated *Pbs21*(−) parasites [9] and used them for this study. It is known that *Pbs21*(−) parasites develop normally in the blood stages and show normal infectivity for mosquitoes and transmission to mice [9, 10]. *Anopheles stephensi* mosquitoes were fed on infected mice carrying either *PbGCS1*(−) or *Pbs21*(−) parasites, which were then dissected for the evaluation of parasite development at day 16 postfeeding. Three independent experiments showed that oocysts (in the midgut) and sporozoites (in the salivary glands) were detected in the mosquitoes fed on mice carrying *Pbs21*(−) parasites. In sharp contrast, no oocyst nor sporozoite was detected in the mosquitoes fed on mice carrying *PbGCS1*(−) parasites (Figures 3E and 3F and Table S2). When naive mice were subjected to these mosquitoes' bites, only *Pbs21*(−) parasites appeared in the mouse blood, indicating that development of *PbGCS1*(−) parasites was completely halted at the mosquito stage (Figure 3E and Table S2). These results indicate that PbGCS1 is essential for the mosquito stages of development.

In *P. berghei*, an in vitro assay has been established that mimics the gametogenesis and fertilization taking place in the mosquito body [6]. By using this system, it was found that the efficiency of male gametogenesis in *PbGCS1*(−) parasites was comparable to that of *Pbs21*(−) parasites (Figure 4A and Table S1). In *Pbs21*(−) parasites, female gametes fertilized with male gametes and then transformed into ookinetes (Figure 4A). In *PbGCS1*(−) parasites, on the other hand, female gametes did not fertilize with males, resulting in 86% of female gametes, which were forming clumps, remaining unfertilized (Figures 4A and 4C). These results clearly indicate that PbGCS1 is involved in the interaction process between male and female gametes.

PbGCS1 Determines Male Fertility of Parasites

As shown in the analysis based on AGFP marker lines, PbGCS1 is expressed in the male gametocytes and gametes. Therefore, the fertilization failure observed in *PbGCS1*(−) parasites likely was attributed to male sterility. To confirm this possibility, we performed two sets of in vitro crossfertilizations between *PbGCS1*(−) and *Pbs21*(−) gametes and two sets of self-fertilizations of *Pbs21* (−) and *PbGCS1* (−) gametes as control experiments. Control experiments showed that self-fertilization of *PbGCS1*(−) parasites did not produce any ookinetes, whereas that of *Pbs21*(−) parasites did (Figure 4B). Because the *Pbs21*gene is inactive in *Pbs21*(−) parasites, ookinetes generated from *Pbs21*(−) self-fertilization did not express Pbs21 protein, which was confirmed by immunostaining (Figure 4B and left panels in Figure 4D). As in the first crossfertilization experiment, *PbGCS1*(−) female gametes were crossed with *Pbs21*(−) male/female gametes. As a result,

Please cite this article in press as: Hirai et al., Male Fertility of Malaria Parasites Is Determined by GCS1, a Plant-Type Reproduction Factor, Current Biology (2008), doi:10.1016/j.cub.2008.03.045

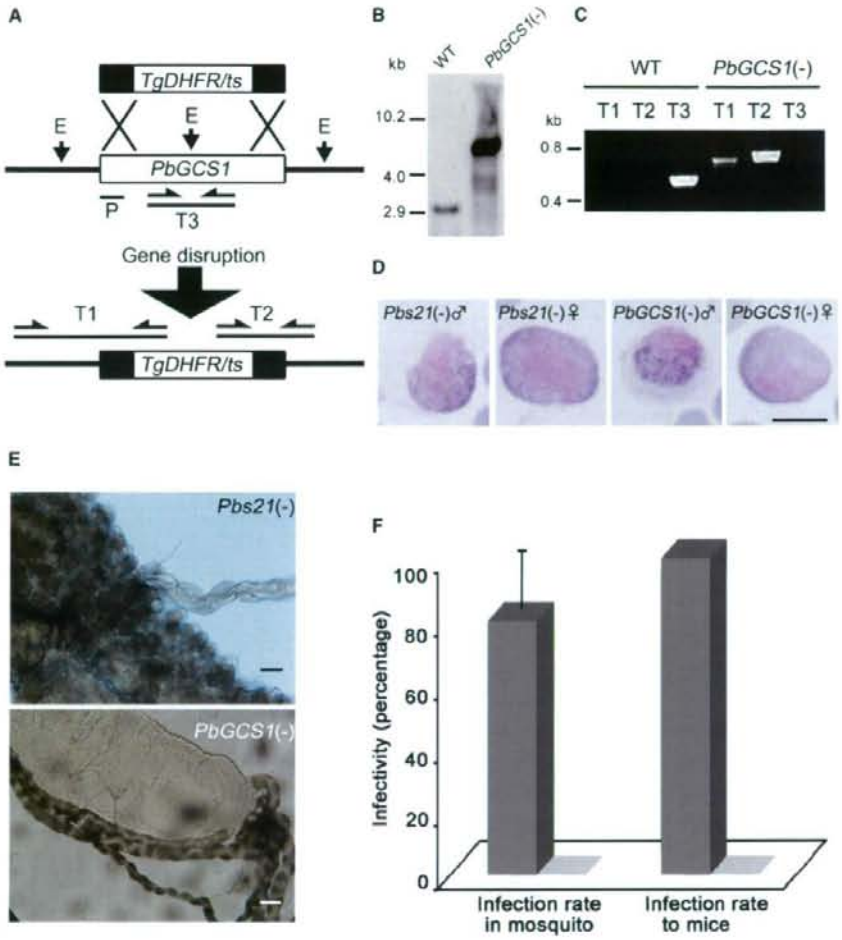

Figure 3. Targeted Disruption of the *PbGCS1* Gene and Resulting Phenotypes of *PbGCS1*(−) *P. berghei*

(A) Schematic representation of replacement strategy to generate *PbGCS1*(−) parasites. The WT *PbGCS1* genomic locus is replaced with 5′ and 3′ regions of *PbGCS1*(−) open reading frame and *TgDHFR*, a selectable marker. "E" and "P" indicate EcoRI sites and the probe region used for the Southern blot analysis shown in (B), respectively. The bars labeled with T1-3 indicate amplified regions by the diagnostic PCRs in (C).

(B) Southern blot analysis of WT and *PbGCS1*(−) parasites.

(C) Diagnostic PCRs. The bands in T1/T2 and T3 are specific to *PbGCS1*(−) and WT parasites, respectively.

(D) *PbGCS1*(−) and *Pbs21*(−) gametocytes were stained with Giemsa. Bar represents 5 μm.

(E) Mosquito midguts infected with *Pbs21*(−) and *PbGCS1*(−) parasites. The latter carries no oocyst. Bars represent 50 μm.

(F) The infection rate and transmission efficiency of *Pbs21*(−) (dark gray bar) and *PbGCS1*(−) (light gray bar). Error bars represent mean ± SD (n = 3). The details are shown in Table S2.

Pbs21-positive (55%) and -negative (45%) ookinetes were produced (Figure 4B and right panels in Figure 4D). In this experiment, Pbs21-negative ookinetes were derived from self-fertilization of *Pbs21*(−) gametes, whereas Pbs21-positive ookinetes were only produced by crossfertilization between *PbGCS1*(−) (namely *Pbs21*[+]) females and *Pbs21*(−) (namely *PbGCS1*[+]) males. This result indicates that *PbGCS1*(−) female gametes are fertile and that disruption of the *PbGCS1* gene does not affect the parasite development after fertilization. As the second crossfertilization experiment, *PbGCS1*(−) male/female gametes were crossed with *Pbs21*(−) females, resulting in no ookinetes (Figure 4B and Table S3). This indicates that *PbGCS1*(−) males failed to fertilize with Pbs21(−) females. The fertilization failure of *PbGCS1*(−) males was not complemented by *Pbs21*(−) (namely *PbGCS1*[+]) females (the results of the in vitro fertilization assay are summarized in Figure S2). We tested the possibility that PbGCS1 may have a role in flagellum motility. The *PbGCS1*(−)

Please cite this article in press as: Hirai et al., Male Fertility of Malaria Parasites Is Determined by GCS1, a Plant-Type Reproduction Factor, Current Biology (2008), doi:10.1016/j.cub.2008.03.045

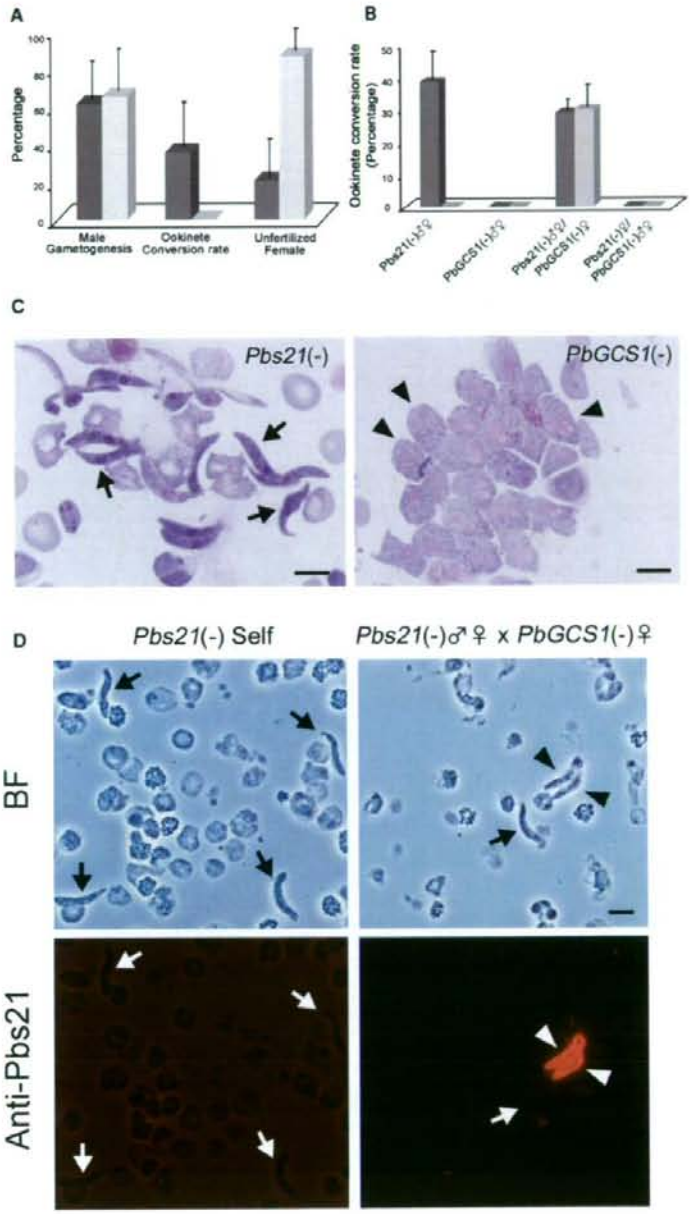

Figure 4. Fertility of *PbGCS1*(−) Parasites

(A) The rates of ♂ gametogenesis, ookinete formation, and unfertilized ♀ gametes of *PbGCS1*(−) (light gray bar) and *Pbs21*(−) (dark gray bar) are indicated. Error bars represent mean ± SD (n = 3). The details are shown in Table S1.

(B) The Pbs21-negative (dark gray bar) and -positive (light gray bar) ookinetes resulting from each mating combination were counted. *Pbs21*(−)♂♀ and *PbGCS1*(−)♂♀ indicate self-fertilization of each line. Error bars represent mean ± SD (n = 3). The details are shown in Table S3.

(C) Transgenic parasites cultured for 16 hr after gametogenesis induction were stained with Giemsa. Many ookinetes were observed in *Pbs21*(−) (exemplified by arrow in left panel), whereas clumps of unfertilized ♀ gametes with no ookinete are seen in *PbGCS1*(−) (arrowhead in right panel). Bars represent 5 μm.

(D) Ookinetes produced by *Pbs21*(−) self-fertilization (left panels) and those by crossfertilization of *PbGCS1*(−) ♀ and *Pbs21*(−) ♂/♀ gametes (right panels) were immunostained with anti-Pbs21 antibody. *Pbs21*(−) ookinetes (indicated with arrows in the left panels) do not show fluorescent signal for Pbs21. Both Pbs21-positive (arrowheads in the right panels) and -negative (arrow in the right panels) ookinetes are produced by crossfertilization. Bars represent 5 μm.

male gametes showed flagella motility and adhesion to surrounding erythrocytes, forming exfagellating centers, all of which were comparable to that of *Pbs21*(−) gametes. However, no successful entering of flagella into female gametes was observed in *PbGCS1*(−) (Movies S1 and S2). Taken together, we conclude that PbGCS1 has a male-specific function during the interaction with female gametes, and, therefore, that PbGCS1 is indispensable for parasite fertilization.

GCS1-Based Fertilization May Be Highly Conserved in Various Organisms

In the present report, we show that PbGCS1, which was initially identified as a putative ortholog to angiosperm GCS1, is surely functional in malaria parasite reproduction. This demonstrates that mechanisms for parasite fertility are, at least in part, common to that of plant fertilization. It is widely accepted that the phylum Apicomplexa, including malaria parasites, is evolved from secondary endosymbiosis of red algae, from which malaria parasites acquired plastids, nonphotosynthetic chloroplasts called "apicoplasts" [11]. Some basic metabolic pathways of malaria parasites (for example, fatty acid synthesis and ferredoxin-dependent redox systems) are encoded by the apicoplast genome. These processes, therefore, show plant-type characteristics derived from red algal plastid metabolisms [12]. The parasite reproduction based on GCS1 probably is not derived from the engulfed red alga because we could not detect any remarkable close relationships of *GCS1* genes between Apicomplexa and red algae in the phylogenetic analysis (Figure 1C). However, it is still possible that the fast-evolving apicomplexan genes mislead their position in the phylogenetic tree. Nevertheless, putative GCS1 orthologs also exist in amoebozoan and opisthokont species, which have not experienced the primary endosymbiosis of cyanobacteria nor secondary endosymbiosis of eukaryotic algae [13] (Figures

Please cite this article in press as: Hirai et al., Male Fertility of Malaria Parasites Is Determined by GCS1, a Plant-Type Reproduction Factor, Current Biology (2008), doi:10.1016/j.cub.2008.03.045

1B and 1C), suggesting that the ancestor of malaria parasites already had the *GCS1* gene before the acquisition of the apicoplast by the red algal secondary endosymbiosis. Given that both plant and apicomplexan *GCS1* genes are involved in fertilization, it is most likely that the original function of GCS1 was in the fertilization of the ancestral eukaryotes.

Besides the conservation of GCS1 possession, our previous study has shown that *C. reinhardtii* and *P. polycephalum* display gamete-specific GCS1 expression at the transcription level, and the expression is dramatically reduced after mating in both organisms [3]. The similar expression pattern also was confirmed in PbGCS1, where the PbGCS1::AGFP protein is expressed in male gametocytes and gametes and the expression is reduced in ookinetes, a postfertilization stage. Such a similarity in stage-specific expression of GCS1 in malaria parasites, plants, algae, and slime mold strongly suggests that GCS1 may function in a similar fashion in these organisms. If this is the case, comparative studies of GCS1 in each organism will accelerate our understanding of the mechanisms involved in fertilization. In addition, there is urgent need for effective strategies to attack parasites threatening humans. The mosquito-parasite interaction has been recognized as a target of transmission-blocking strategies. Several candidate molecules involved in this interaction have been found in gametes, zygotes, and ookinetes and have been tested for their ability to block transmission [2]. For this purpose, the gametic interaction is a novel target. It is worth exploring the possibility of whether GCS1-attacking approaches could be a new antiparasite strategy without affecting the host's reproduction because an obvious GCS1 homolog has not been detected in mammalians.

Experimental Procedures

Plasmid Construction

Procedures for construction of *PbGCS1::AGFP* and *PbGCS1prom::AGFP* plasmids, and primer sequences used in this study are described in the Supplemental Data.

Generation of *PbGCS1* Knockout Parasites

For disruption of *PbGCS1*, two *P. berghei* (ANKA clone 2.34) genomic fragments covering the *PbGCS1* coding region were amplified with two sets of primers (GCS1-F1-HindIII/GCS1-R1-HindIII and GCS1-F2-EcoRI/GCS1-R2-BamHI). Cloning these fragments into the *P. berghei* targeting vector pBS-DHFR [14] resulted in the plasmid pPbGCS1-KO. The transfection, pyrimethamine selection, and dilution cloning were performed as described [15]. Three *PbGCS1*(−) clones (1–3, 2–5, and 3–6) from three independent transfection experiments were obtained. The expected recombination event in each clone was confirmed by diagnostic PCR. For Southern blot analyses, a DNA fragment amplified with primers (PbGCS1-F1/PbGCS1-R1) and *P. berghei* genomic DNA was labeled with AlkPhos Direct Labeling Kit (GE Healthcare Bioscience) and used as a probe.

Assessment of Blood Stage Development and Fertility

Thin blood films prepared from mice infected with either *PbGCS1*(−) or *Pbs21*(−) parasites were stained with Giemsa, on which parasitemia, gametocytemia, and sex ratio were calculated. To evaluate the efficiency of fertilization and subsequent development into ookinetes, infected blood was mixed with gametogenesis-inducing medium to induce gamete formation; then, the number of exflagellating males was counted at 15 min after induction. The sample was further cultured for 16 hr, when the number of ookinetes was counted. Sex-specific involvement of PbGCS1 in sexual reproduction was analyzed by a crossfertilization assay as described below.

Infectivity of Parasite for Mosquitos and Transmission to Mice

Anopheles stephensi were reared as previously described [16] and infected with parasites as described [5]. In brief, female mosquitoes (4–7 days old) were fed on mice carrying either *Pbs21*(−) or *PbGCS1*(−) parasites, and fully engorged mosquitoes were collected. Sixteen days after blood feeding, ten mosquitoes were dissected, and midguts and salivary glands were isolated. The number of oocysts on the midgut and the presence of sporozoites in the salivary glands was examined. The rest of the mosquitoes were fed on naive Balb/c mice. The transmission of parasites from mosquitoes to mice was examined by checking mouse blood smears every day for 2 weeks after the feeding.

In Vitro Crossfertilization Assay

The in vitro crossfertilization assay was performed as previously described [6]. Five μl of tail blood from a mouse infected with parasite clone A (*PbGCS1*[−] or *Pbs21*[−] parasites) was immediately added to 1 ml of gametogenesis-inducing medium (10% fetal bovine serum in RPMI1640, pH 8.2) containing 500 μM of aphidicolin at 21°C for 12 min to induce female gamete formation. Aphidicolin inhibits male gamete formation, whereas female gametes are formed normally. At the same time, 5 μl of tail blood from a mouse infected with clone B (*PbGCS1*[−] or *Pbs21*[−] parasites) was added immediately into 1 ml of gametogenesis-inducing medium at 21°C for 12 min without aphidicolin. Clone A was centrifuged, and the supernatant removed. The suspension of clone B was added to the pellet of clone A and mixed. This mixture was further incubated for 16 hr to induce fertilization and ookinete formation. The ookinete conversion rate was determined by the percentage of female gametocytes of clone A that fertilized with male gametes of clone B and transformed into ookinetes. Ookinetes were immunostained with anti-Pbs21 monoclonal antibody as described in the Supplemental Data.

Accession Numbers and Phylogenetic Study

See the Accession Numbers section for information on the *PbGCS1* cDNA sequence. The accession numbers of other GCS1s are *C. parvum* (XP_627125), *T. thermophila* (XP_001030543), *P. tetraurelia* (XP_001431224), *T. cruzi* (XP_814894), *T. brucei* (XP_823296), *L. infantum* (XP_001468864), *L. major* (XP_843157), *C. merolae* (AP006493), *P. polycephalum* (BAE71144), *L. longiflorum* (BAE71142), *A. thaliana* (BAE71143), *O. stiva* (NP_001055054), *C. reinhardtii* (XP_001695893). *V. vinifera* (CAO63696), *P. patens* (XP_001770778), *M. brevicollis* (XP_001746497), *H. magnipapillata* (ABN45755), *N. vectensis* (XP_001628495), and *D. discoideum* (Dd1, XP_643321; Dd2, AAS45348). Phylogenetic analysis using these sequences is described in the Supplemental Data.

Accession Numbers

The GenBank accession number for the *PbGCS1* cDNA sequence reported in this paper is EU369602.

Supplemental Data

Supplemental Experimental Procedures, two figures, three tables, and two movies are available at http://www.current-biology.com/cgi/content/full/18/8/■■■/DC1/.

Acknowledgments

This research was supported by a Grant-in-Aid for Young Scientists (B) (M.H.), for Exploratory Research (M.A.), and for Scientific Research (B) (H.M.) from the Japan Society for the Promotion of Science, the Special Postdoctoral Researchers Program of Riken (T.M.), the Program for the Promotion of Basic Research Activities for Innovative Biosciences (T.K.), and Creative Scientific Research from the Japanese Ministry of Education, Science, Culture, Sports, and Technology (K.K.).

Received: February 8, 2008
Revised: March 10, 2008
Accepted: March 20, 2008
Published online: April 10, 2008

References

1. Baton, L.A., and Ranford-Cartwright, L.C. (2005). Spreading the seeds of million-murdering death: metamorphoses of malaria in the mosquito. Trends Parasitol. *21*, 573–580.
2. Sauerwein, R.W. (2007). Malaria transmission-blocking vaccines: the bonus of effective malaria control. Microbes Infect. *9*, 792–795.

Please cite this article in press as: Hirai et al., Male Fertility of Malaria Parasites Is Determined by GCS1, a Plant-Type Reproduction Factor, Current Biology (2008), doi:10.1016/j.cub.2008.03.045

3. Mori, T., Kuroiwa, H., Higashiyama, T., and Kuroiwa, T. (2006). GENERATIVE CELL SPECIFIC 1 is essential for angiosperm fertilization. Nat. Cell Biol. *8*, 64–71.
4. von Besser, K., Frank, A.C., Johnson, M.A., and Preuss, D. (2006). Arabidopsis HAP2 (GCS1) is a sperm-specific gene required for pollen tube guidance and fertilization. Development *133*, 4761–4769.
5. Hirai, M., Arai, M., Kawai, S., and Matsuoka, H. (2006). PbGCβ is essential for Plasmodium ookinete motility to invade midgut cell and for successful completion of parasite life cycle in mosquitoes. J. Biochem. (Tokyo) *140*, 747–757.
6. van Dijk, M.R., Janse, C.J., Thompson, J., Waters, A.P., Braks, J.A., Dodemont, H.J., Stunnenberg, H.G., van Gemert, G.J., Sauerwein, R.W., and Eling, W. (2001). A central role for P48/45 in malaria parasite male gamete fertility. Cell *104*, 153–164.
7. Winger, L.A., Tirawanchai, N., Nicholas, J., Carter, H.E., Smith, J.E., and Sinden, R.E. (1988). Ookinete antigens of Plasmodium berghei. Appearance on the zygote surface of an Mr 21 kD determinant identified by transmission-blocking monoclonal antibodies. Parasite Immunol. *10*, 193–207.
8. Paton, M.G., Barker, G.C., Matsuoka, H., Ramesar, J., Janse, C.J., Waters, A.P., and Sinden, R.E. (1993). Structure and expression of a post-transcriptionally regulated malaria gene encoding a surface protein from the sexual stages of Plasmodium berghei. Mol. Biochem. Parasitol. *59*, 263–275.
9. Tomas, A.M., Margos, G., Dimopoulos, G., van Lin, L.H.M., de Koning-Ward, T.F., Sinha, R., Lupetti, P., Beetsma, A.L., Rodriguez, M.C., Karras, M., et al. (2001). P25 and P28 proteins of the malaria ookinete surface have multiple and partially redundant functions. EMBO J. *20*, 3975–3983.
10. Sidén-Kiamos, I., Vlachou, D., Margos, G., Beetsma, A., Waters, A.P., Sinden, R.E., and Louis, C. (2000). Distinct roles for pbs21 and pbs25 in the in vitro ookinete to oocyst transformation of Plasmodium berghei. J. Cell Sci. *113*, 3419–3426.
11. Foth, B.J., and McFadden, G.I. (2003). The apicoplast: a plastid in Plasmodium falciparum and other Apicomplexan parasites. Int. Rev. Cytol. *224*, 57–110.
12. Kimata-Ariga, Y., Kurisu, G., Kusunoki, M., Aoki, S., Sato, D., Kobayashi, T., Kita, K., Horii, T., and Hase, T. (2007). Cloning and characterization of ferredoxin and ferredoxin-NADP+ reductase from human malaria parasite. J. Biochem. (Tokyo) *141*, 421–428.
13. Reyes-Prieto, A., Weber, A.P., and Bhattacharya, D. (2007). The origin and establishment of the plastid in algae and plants. Annu. Rev. Genet. *41*, 147–168.
14. Dessens, J.T., Beetsma, A.L., Dimopoulos, G., Wengelnik, K., Crisanti, A., Kafatos, F.C., and Sinden, R.E. (1999). CTRP is essential for mosquito infection by malaria ookinetes. EMBO J. *18*, 6221–6227.
15. Janse, C.J., Ramesar, J., and Waters, A.P. (2006). High-efficiency transfection and drug selection of genetically transformed blood stages of the rodent malaria parasite Plasmodium berghei. Nat. Protocols *1*, 346–356.
16. Hirai, M., Wang, J., Yoshida, S., Ishii, A., and Matsuoka, H. (2001). Characterization and identification of exflagellation-inducing factor in the salivary gland of Anopheles stephensi (Diptera: Culicidae). Biochem. Biophys. Res. Commun. *287*, 859–864.

Coinfection with Nonlethal Murine Malaria Parasites Suppresses Pathogenesis Caused by *Plasmodium berghei* NK65

Mamoru Niikura,[1]*‡ Shigeru Kamiya,† Kiyoshi Kita,‡ and Fumie Kobayashi[1]†

Mixed infection with different *Plasmodium* species is often observed in endemic areas, and the infection with benign malaria parasites such as *Plasmodium vivax* or *P. malariae* has been considered to reduce the risk of developing severe pathogenesis caused by *P. falciparum*. However, it is still unknown how disease severity is reduced in hosts during coinfection. In the present study, we investigated the influence of coinfection with nonlethal parasites, *P. berghei* XAT (*Pb* XAT) or *P. yoelii* 17X (*Py* 17X), on the outcome of *P. berghei* NK65 (*Pb* NK65) lethal infection, which caused high levels of parasitemia and severe pathogenesis in mice. We found that the simultaneous infection with nonlethal *Pb* XAT or *Py* 17X suppressed high levels of parasitemia, liver injury, and body weight loss caused by *Pb* NK65 infection, induced high levels of reticulocytemia, and subsequently prolonged survival of mice. In coinfected mice, the immune response, including the expansion of $B220^{int}CD11c^{+}$ cells and $CD4^{+}$ T cells and expression of IL-10 mRNA, was comparable to that in nonlethal infection. Moreover, the suppression of liver injury and body weight loss by coinfection was reduced in IL-$10^{-/-}$ mice, suggesting that IL-10 plays a role for a reduction of severity by coinfection with nonlethal malaria parasites. *The Journal of Immunology*, 2008, 180: 6877–6884.

Malaria is the infectious disease that causes incidence estimates of 2–3 million deaths and 300–500 million clinical cases in the world (1). There are four species of *Plasmodium* that infect humans: *Plasmodium falciparum*, *Plasmodium vivax*, *Plasmodium malariae*, and *Plasmodium ovale*. *P. falciparum* is the major human parasite responsible for high morbidity and mortality, and infection with *P. falciparum* is associated with developing fever, a high number of parasites in the blood, and pathogenesis, including severe anemia, body weight loss, and cerebral malaria in humans (2). The sensitive PCR-based techniques have revealed that coinfection with different *Plasmodium* species is common in developing countries (3, 4). In particular, the simultaneous presence of *P. vivax* or *P. malariae* during *P. falciparum* infection is often observed when the prevalence of *Plasmodium* infections in humans is analyzed in endemic areas (5–7) and it is known to reduce the risk of developing a high number of parasites in the blood as well as pathogenesis (8–11).

Murine malaria models have been used for understanding the induction of immune interaction in hosts and investigating factors associated with malarial defense mechanism. Coinfection with two different species and/or strains of murine malaria parasites has been shown to influence the parasitemia or mortality of each other (12). The development of experimental cerebral malaria caused by *Plasmodium berghei* (*Pb*)[2] ANKA was inhibited by the simultaneous presence of *Plasmodium yoelii yoelii* or *P. berghei* K173 (13, 14). However, it is still unknown how the disease severity is suppressed in simultaneous infection.

In the present study, we investigated the influence of simultaneous infection with nonlethal parasites, *P. berghei* XAT (*Pb* XAT) or *P. yoelii* 17X (*Py* 17X), on the outcome of *P. berghei* NK65 (*Pb* NK65) lethal infection, which causes high levels of parasitemia and pathogenesis such as body weight loss and liver injury in mice. First, we found that *Pb* XAT-immunized mice acquired resistance to *Pb* NK65 infection, although *Py* 17X-immunized mice were susceptible to *Pb* NK65 infection. By using these three species and strains, we examined how *Pb* XAT or *Py* 17X nonlethal infection modulated the immune responses such as cytokine production and cellular expansion during *Pb* NK65 lethal infection.

Materials and Methods

Mice

Female C57BL/6 (B6) mice were purchased from CLEA Japan and used at 5–6 wk of age. IL-$10^{-/-}$ mice on B6 background were purchased from The Jackson Laboratory. We used 20- to 24-wk-old female IL-$10^{-/-}$ mice (experiment 1), 5- to 6-wk-old male or female IL-$10^{-/-}$ mice (experiment 2), and age-matched female B6 mice in these studies. The genotype of female IL-$10^{-/-}$ mice used in experiments was verified by PCR. The experiments were approved by the Experimental Animal Ethics Committee at Kyorin University, and all experimental animals were kept on the specific pathogen-free unit at the animal facility with sterile bedding, food, and water.

Parasites and infections

Malaria parasites were stored as frozen stocks in liquid nitrogen. *Pb* NK65 is a high-virulence strain and was originally obtained from Dr. M. Yoeli (New York University Medical Center, New York, NY). *Pb* XAT is a low-virulence derivative from *Pb* NK65 (15). A nonlethal isolate of *Py* 17X was originally obtained from Dr. J. Finnerty (National Institutes of Health, Bethesda, MD) and cloned by limiting dilution. Parasitized RBCs (pRBCs) of *Pb* NK65, *Pb* XAT, and *Py* 17X were generated in donor mice inoculated i.p. with each frozen stock of parasites. The donor mice were monitored for parasitemia daily and bled for experimental infection in ascending periods of parasitemia. Experimental mice were infected i.v. with 1×10^4 pRBCs of a given parasite species or strain. Therefore, when mice were coinfected with two species/strains of parasites, a total of 2×10^4 pRBCs (1×10^4 of each parasite species/strain) were inoculated.

*Institute of Laboratory Animals, Graduate School of Medicine and †Department of Infectious Diseases, Faculty of Medicine, Kyorin University, Tokyo; and ‡Department of Biomedical Chemistry, Graduate School of Medicine, University of Tokyo, Tokyo, Japan

Received for publication July 12, 2007. Accepted for publication March 4, 2008.

The costs of publication of this article were defrayed in part by the payment of page charges. This article must therefore be hereby marked *advertisement* in accordance with 18 U.S.C. Section 1734 solely to indicate this fact.

[1] Address correspondence and reprint requests to Dr. Fumie Kobayashi and Dr. Mamoru Niikura, Faculty of Medicine, Kyorin University, 6-20-2 Shinkawa, Mitaka, Tokyo 181-8611, Japan. E-mail addresses: fumfum@ks.kyorin-u.ac.jp and mniikura@ks.kyorin-u.ac.jp

[2] Abbreviations used in this paper: *Pb*, *Plasmodium berghei*; *Py*, *Plasmodium yoelii*; pRBC, parasitized RBC; AST, aspartic aminotransferase; ALT, alanine aminotransferase.

Table I. *Total spleen cell number in uninfected and infected mice ($\times 10^8$)*[a]

	Days Postinfection			
	0	6	9	15
Uninfected	0.35 ± 0.17			
Pb NK65		1.05 ± 0.16	0.62 ± 0.25	
Pb XAT		0.74 ± 0.08	2.94 ± 0.75	4.41 ± 1.61
Pb NK65/*Pb* XAT		0.74 ± 0.10	2.22 ± 0.70	6.52 ± 0.98
Py 17X		0.99 ± 0.18	4.63 ± 0.77	10.4 ± 3.02
Pb NK65/*Py* 17X		1.28 ± 0.02	4.63 ± 1.34	11.6 ± 3.48

[a] Mice were infected with malarial parasites as described in the legend to Fig. 2. Spleens were obtained from uninfected and infected mice on days 6, 9, and 15 after infection. Results are expressed as means ± SD of three mice. Experiments were performed three times with similar results.

Parasitemia

Parasitized RBCs were observed by microscopic examination of methanol-fixed tail blood smears stained for 45 min with 1% Giemsa diluted in phosphate buffer (pH 7.2). The number of pRBCs in 250 RBCs was enumerated when parasitemia exceeded 10%, whereas 1×10^4 RBCs were examined when mice showed lower parasitemia. The percentage of parasitemia was calculated as follows: [(No. of pRBCs)/(Total no. of RBCs counted)] × 100.

Measurement of body weights, hematocrits, and circulating reticulocytes

Body weights were measured by balance for animals (KN-661; Natume), and body weight loss was expressed as a percentage of the day 0 value. For hematocrit measurement, tail blood (50 μl) was collected into a heparinized capillary tube and centrifuged at 13,000 × rpm for 5 min with a micro hematocrit centrifuge (HC-12A; Tomy). The hematocrit value was expressed as a percentage of the total blood volume. Reticulocytes in 250 RBCs were counted when reticulocytemia exceeded 20%, whereas 1×10^4 RBCs were examined when mice showed lower reticulocytemia. The percentage of reticulocytemia was calculated as follows: [(No. of reticulocytes)/(Total no. of RBCs counted)] × 100.

Histological examination and measurement of parameters of liver injury

Livers were obtained from infected mice on day 9 postinfection and fixed in 10% buffered formalin and embedded in paraffin. Six-micrometer-thick sections were stained with H&E. The blood was obtained from infected mice on day 9 and centrifuged at 500 × *g* for 10 min. The resulting supernatants were stored at −20°C and used as plasma. The levels of aspartic aminotransferase (AST) and alanine aminotransferase (ALT) in plasma were determined at Nagahama Life Science Laboratory (Shiga, Japan).

Flow cytometry

Flow cytometric analysis was performed on single-cell suspensions of spleen and peripheral blood cells as described previously (16). Total spleen cell numbers in uninfected and infected mice are shown in Table I. The following mAbs were used for analysis: FITC-conjugated anti-CD3ε mAb (clone 145-2C11; eBioscience) and anti-CD4 mAb (clone RM4–5; eBioscience); PE-conjugated anti-CD11c mAb (clone N418; Miltenyi Biotec); allophycocyanin-conjugated anti-CD3ε mAb (clone 145–2C11; eBioscience); and biotin-conjugated anti-CD45R mAb (B220; clone RA3–6B2; BD Pharmingen). MAbs were added to cells in FACS buffer (1% BSA, 0.1% sodium azide in PBS) and incubated at 4°C for 30 min and the cells were washed with cold FACS buffer by centrifugation at 250 × *g* for 2 min. Biotinylated mAbs were followed by streptavidin-conjugated allophycocyanin (4°C, 30 min). After washing with FACS buffer, cells were fixed with 1% paraformaldehyde. Two-color flow cytometry was performed and analyzed with a FACSCalibur (BD Biosciences) using a FlowJo software (version 7.1.3, for Windows).

Detection of cytokine mRNA in spleens

Spleens were removed from infected mice on day 9 postinfection and total RNA was isolated by Isogen (Nippon Gene) according to the manufacturer's protocol. The splenic RNA was reverse-transcribed by murine leukemia virus reverse transcriptase (Applied Biosystems) using random hexamer primers, and reverse transcriptase reaction was preformed at 70°C for 10 min, at 25°C for 10 min, and at 42°C for 30 min. The reaction was terminated by heating at 99°C for 5 min, and the cDNA products were stored at −20°C until use. The 50 μl PCR mixture contained 1 × TaKaRa Ex *Taq* buffer, 2.5 mM dNTP, 1 μl cDNA products, 5 U/μl TaKaRa Ex *Taq* DNA polymerase, and 0.25 μM of PCR primers. The primers used for PCR amplification were as follows: IL-10, 5′-GTG AAG ACT TTC TTT CAA ACA AAG, 3′-CTG CTC CAC TGC CTT GCT CTT ATT; IFN-γ, 5′-TAC TGC CAC GGC ACA GTC ATT GAA, 3′-GCA GCG ACT CCT TTT CCG CTT CCT T; β-actin, 5′-CCA GCC TTC CTT CCT GGG TA, 3′-CTA GAA GCA TTT GCG GTG CA. Thirty cycles of PCR were performed on a thermal cycler (iCycler; Bio-Rad). Each cycle consisted of 30 s of denaturation at 94°C, 30 s of annealing at 60°C, and 1 min of extension at 72°C. The PCR products were analyzed on a 2% agarose gel stained with ethidium bromide.

Cytokine assay

An ELISA for the detection of IFN-γ or IL-10 in plasma was conducted as described previously (16). A rat anti-mouse IFN-γ (clone R4–6A2; eBioscience) and a rat anti-mouse IL-10 (clone JES5–16E3; eBioscience) were used as the capture Abs, and a biotin-coupled rat anti-mouse IFN-γ (clone XMG1.2; eBioscience) and IL-10 (clone JES5-2A5; eBioscience) were used as the detecting Abs. The concentration of cytokines in plasma was calculated from standard curves prepared with known quantities of murine recombinant IFN-γ (Genzyme) and murine recombinant IL-10 (Pierce).

Statistical analysis

For time-series comparisons, Student's *t* test and one- and two-way ANOVAs with Fisher's PLSD post hoc test were performed using Statcel program (OMS). Survival curves were compared using a log-rank test. $p < 0.05$ was set as statistical significance of differences.

Results

Infection with Pb *XAT but not* Pb *17X induces protective immunity to* Pb *NK65*

It has been shown that mice infected with *Pb* NK65 develop severe parasitemia and die within 2 wk, although mice infected with *Pb* XAT or *Py* 17X cure spontaneously around 3 wk of infection (15, 17). To examine whether primary infection with each of the two nonlethal parasites can induce protective immunity against *Pb* NK65 lethal infection, groups of C57BL/6 (B6) mice were infected with *Pb* XAT or *Py* 17X then challenged with *Pb* NK65 on day 30 after primary infection. As expected, mice cured from *Pb* XAT infection (*Pb* XAT-immunized mice) showed extremely low levels of parasitemia after secondary infection with *Pb* NK65 (Fig. 1*A*). On the contrary, mice cured from *Py* 17X infection (*Py* 17X-immunized mice) showed high levels of parasitemia, with some delay in onset of parasitemia, and eventually died after *Pb* NK65 infection (Fig. 1*B*). These results suggest that protective immunity to *Pb* NK65 is induced by immunizing mice with *Pb* XAT but not with heterologous *Py* 17X.

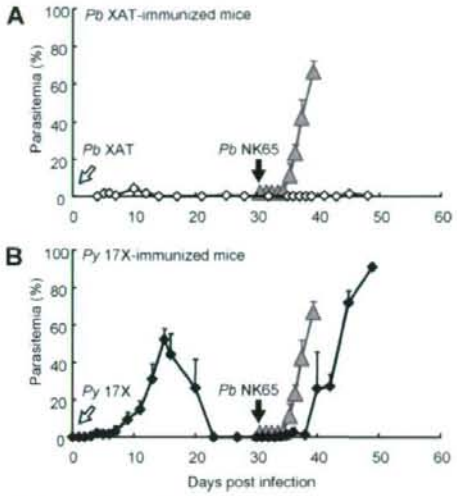

FIGURE 1. Immunization with *Pb* XAT but not *Py* 17X induces protective immunity to *Pbi* NK65. C57BL/6 mice were infected with 1×10^4 pRBCs of *Pb* XAT (*A*) or *Py* 17X (*B*) (day 0, open arrows). On day 30 after primary infection (filled arrows), both groups of mice were challenged with 1×10^4 pRBCs of *Pb* NK65. *A*, Course of parasitemia in immunized mice with *Pb* XAT (◇). *B*, Course of parasitemia in immunized mice with *Py* 17X (◆). Course of parasitemia of unimmunized mice infected with *Pb* NK65 is inserted to figures (shaded triangles). Results are expressed as mean percentage parasitemia ± SD of three mice. Experiments were performed three times with similar results.

The pathogenesis during Pb *NK65 infection is reduced by simultaneous infection with nonlethal malaria parasites*

To investigate whether the existence of nonlethal malaria parasite affects the outcome of *Pb* NK65 infection, B6 mice were infected with *Pb* NK65 and nonlethal parasites simultaneously. When mice were coinfected with *Pb* NK65 and *Pb* XAT (*Pb* NK65/*Pb* XAT), they showed lower levels of parasitemia than did *Pb* NK65 singly infected mice during early infection (Fig. 2*A*) and survived significantly longer than did *Pb* NK65 singly infected mice (Fig. 2*B*) ($p = 0.0013$). Moreover, the body weight loss of the coinfected mice was prevented early in infection (Fig. 2*C*) ($p < 0.0005$ compared with *Pb* NK65-infected mice on days 9–10). Next, we examined the influence of coinfection with nonlethal *Py* 17X on the outcome of *Pb* NK65 infection. Although *Py* 17X immunization did not affect the outcome of *Pb* NK65 infection greatly (Fig. 1*B*), simultaneous infection with *Py* 17X (*Pb* NK65/*Py* 17X) suppressed severe parasitemia, mortality ($p = 0.0005$), and the body weight loss ($p < 0.0005$ on days 6–10) observed in *Pb* NK65 singly infected mice (Fig. 2, *D–F*).

Coinfection with nonlethal malaria parasites induces reticulocytemia

To examine whether the existence of nonlethal malaria parasites affects the severe anemia caused by *Pb* NK65 infection, we determined the hematocrit in mice during *Pb* NK65 single infection and coinfection with *Pb* XAT or *Py* 17X. Coinfection with *Pb* XAT caused acute anemia as severe as did *Pb* NK65 single infection on day 9 postinfection, and the levels of hematocrit were also low on day 15 (Fig. 3*A*). Mice infected with *Pb* XAT did not cause acute severe anemia. In contrast, mice coinfected with *Pb* NK65/*Py* 17X did not cause as severe anemia as for *Pb* NK65-infected mice on day 9, and their reducing pattern of hematocrit was similar to that in *Py* 17X singly infected mice (Fig. 3*C*).

Next, we determined the reticulocytemia in infected mice. *Pb* NK65 singly infected mice did not show any reticulocytemia during infection (Fig. 3*B*). Mice coinfected with *Pb* NK65/*Pb* XAT showed the same levels of reticulocytemia as did *Pb* XAT singly infected mice on day 9 postinfection. However, coinfected mice showed much higher reticulocytemia than that in *Pb* XAT singly infected mice from day 11 postinfection (Fig. 3*B*). As shown in Fig. 3*D*, reticulocytemia in mice coinfected with *Pb* NK65/*Py* 17X increased moderately, and their kinetics were similar to those in *Py* 17X singly infection. These results indicate that the severe anemia caused by *Pb* NK65 infection is suppressed by coinfection with *Py* 17X but not with *Pb* XAT. It is suggested that high levels of reticulocytemia observed during *Pb* NK65/*Pb* XAT infection may

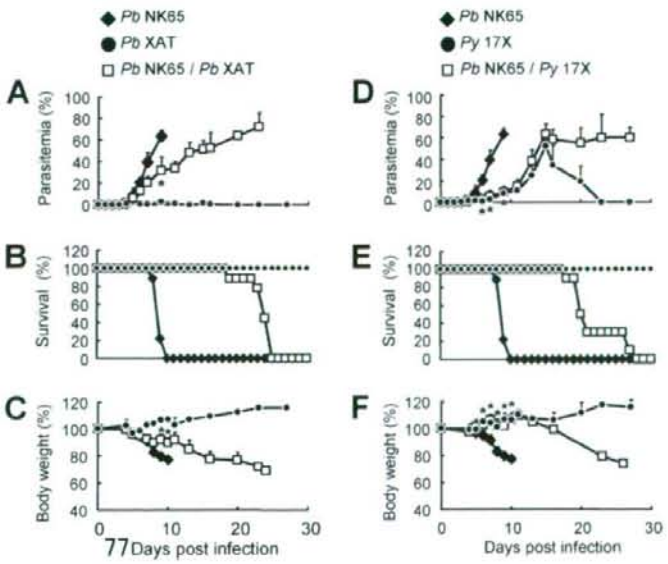

FIGURE 2. Coinfection of nonlethal *Pb* XAT or *Py* 17X suppresses the acute severe parasitemia and body weight loss caused by *Pb* NK65 infection in mice and prolonged their survival. C57BL/6 mice were inoculated with 1×10^4 pRBCs of *Pb* NK65, *Pb* XAT, or *Py* 17X. When mice were coinfected with two species/strains of parasites, a total of 2×10^4 pRBCs were inoculated (*Pb* NK65/*Pb* XAT or *Pb* NK65/*Py* 17X). Results of coinfection are shown for *Pb* NK65/*Pb* XAT (*A–C*) or *Pb* NK65/*Py* 17X (*D* and *E*). *A* and *D*, Course of parasitemia. Asterisks indicate statistically significant differences (*, $p < 0.001$ as compared with *Pb* NK65-infected mice). *B* and *E*, Survival rates. Differences between *Pb* NK65 singly infected mice and coinfected mice are statistically significant ($p < 0.001$). *C* and *F*, Body weights. Asterisks indicate statistically significant differences (*, $p < 0.001$ as compared with *Pb* NK65-infected mice). Results are expressed as means ± SD of five mice. Experiments were performed three times with similar results.

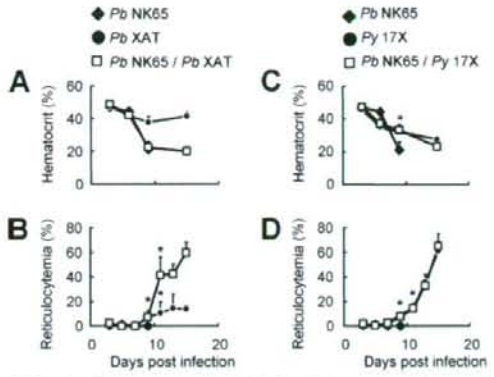

FIGURE 3. Coinfection with nonlethal malaria parasites induces reticulocytemia. Mice were infected with malarial parasites as described in the legend to Fig. 2. *A* and *C*, Blood (50 μl) was collected from infected mice on days 3, 6, 9, and 15 after infection and hematocrit values were determined. *B* and *D*, Reticulocytemia was determined on days 3, 5, 7, 9, 11, 13, and 15 after infection. The percentage of reticulocytemia was calculated as follows: [(number of reticulocytes)/(total number of RBCs counted)] $\times$ 100. Asterisks indicate a statistically significant difference (*, $p < 0.001$ as compared with *Pb* NK65-infected mice). Results are expressed as means $\pm$ SD of three mice. Experiments were performed three times with similar results.

be induced by severe anemia. The different outcome of the suppression of anemia and reticulocytemia between *Pb* NK65/*Pb* XAT- and *Pb* NK65/*Py* 17X-infected mice might be attributed to the difference in parasitemia during early infection.

Low levels of liver injury in mice coinfected with nonlethal malaria parasites

To investigate whether the existence of nonlethal malaria parasites affects the liver injury caused by *Pb* NK65 infection, we performed histological examination of livers from mice during *Pb* NK65 single infection and coinfection with *Pb* XAT or *Py* 17X. As shown in Fig. 4, focal necrosis of the liver cells (Fig. 4, *B* and *F*, arrowheads) and dense infiltration of inflammatory cells such as mononuclear cells around the portal tracts (Fig. 4*F*, arrows) were observed in *Pb* NK65-infected mice. Mice coinfected with *Pb* NK65/*Pb* XAT or *Pb* NK65/*Py* 17X also showed dense infiltration of inflammatory cells (Fig. 4, *G* and *H*, arrows), but focal necroses were not observed in the liver (Fig. 4, *C* and *D*).

We determined the levels of AST and ALT, which are parameters of liver injury, in the plasma. *Pb* NK65-infected mice, in which the focal necroses of liver cells were observed, showed the significantly high concentration of AST and ALT compared with uninfected control mice (Fig. 4, *I* and *J*). The levels of AST and ALT in coinfected mice were quite low and almost the same as those in *Pb* XAT or *Py* 17X singly infected mice.

Coinfection with nonlethal parasites accelerates B220^{int}CD11c^{+} cell expansion in spleen and peripheral blood

To examine the expansion of the CD11c^{+} cell populations during malaria, additional experiments were performed using peripheral blood and spleen obtained from infected mice by flow cytometry in each time point after infection. It was notable that the B220^{int}CD11c^{+} cell population significantly increased in peripheral blood from *Pb* NK65/*Pb* XAT- or *Pb* NK65/*Py* 17X-coinfected mice on day 6 postinfection (Fig. 5*A*, *upper panels*). Their expansion was comparable to that observed in *Pb* XAT or *Py* 17X

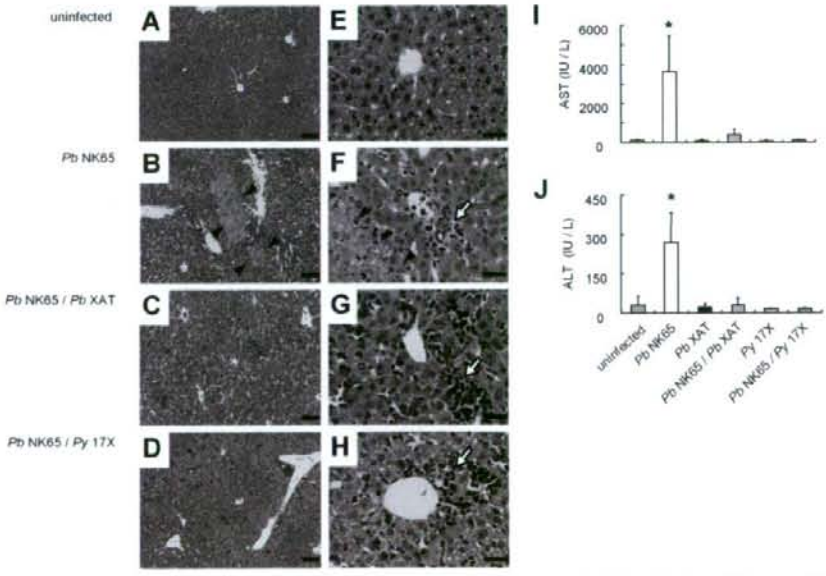

FIGURE 4. The existence of nonlethal malaria parasites prevents the liver injury caused by *Pb* NK65 infection. Mice were infected with malarial parasites as described in the legend to Fig. 2. Livers and plasma were obtained from infected mice on day 9 after infection and from uninfected mice. *A–H*, Histological analysis was performed after staining with H&E. Typical results of uninfected mice (*A* and *E*), mice singly infected with *Pb* NK65 (*B* and *F*), and mice coinfected with *Pb* NK65/*Pb* XAT (*C* and *G*) or *Pb* NK65/*Py* 17X (*D* and *H*) are shown. *A–D*, The scale bar indicates 100 μm. Arrowheads indicate focal necrosis of the liver cells. *E–H*, The scale bar indicates 40 μm. Arrows indicate dense infiltration of inflammatory cells. *I* and *J*, Levels of AST and ALT. Asterisks indicate a statistically significant difference (*, $p < 0.001$ as compared with uninfected control mice). Results are expressed as means $\pm$ SD of three mice. Experiments were performed three times with similar results and the representative data are shown.

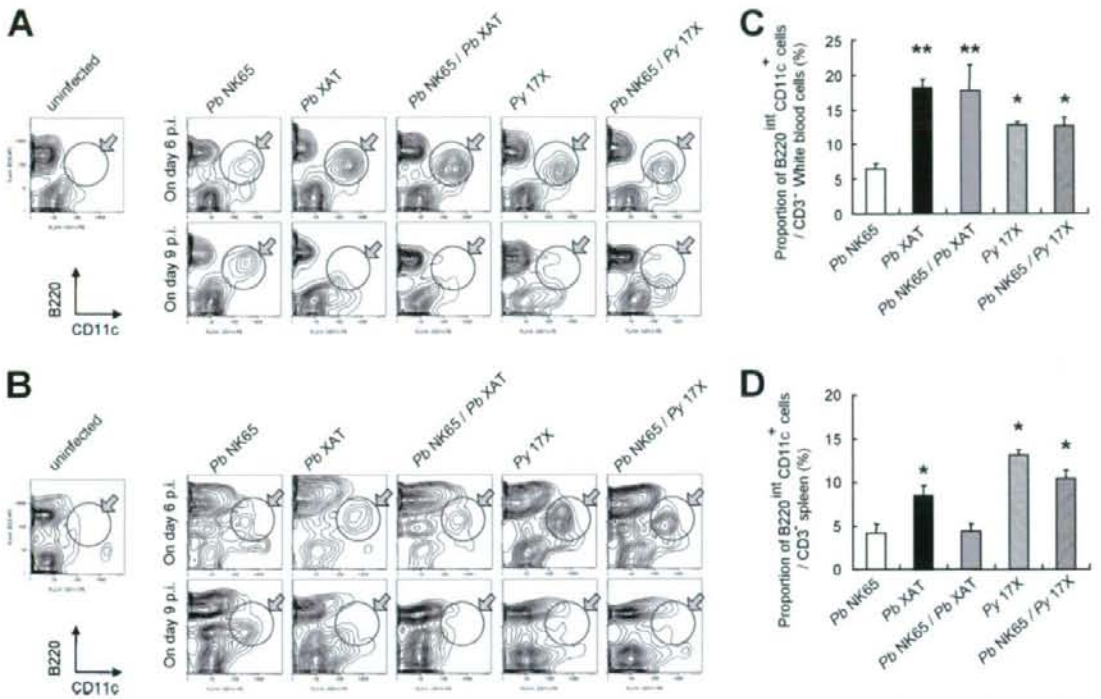

FIGURE 5. Coinfection with nonlethal parasites accelerates $B220^{int}CD11c^+$ cell expansion in spleen and peripheral blood. Peripheral blood and spleen were obtained from infected mice as described in the legend to Fig. 2 on days 6 and 9 after infection and from uninfected mice. Analyses of $CD11c^+$ cell population in peripheral blood (*A* and *C*) and spleen (*B* and *D*) from infected mice were performed by flow cytometery. Expression of B220 and CD11c was analyzed in the gate of $CD3^-$. *A* and *B*, Contour plots of $B220^{int}CD11c^+$ cell population (day 6, *upper panels*; day 9, *lower panels*). p.i., Post infection. Experiments were performed three times with similar results and the representative results are shown. *C* and *D*, The proportion of $B220^{int}CD11c^+$ cells in $CD3^-$ cells is shown (on day 6 postinfection). Asterisks indicate a statistically significant difference (*, $p < 0.005$; **, $p < 0.001$ as compared with *Pb* NK65-infected mice). Results are expressed as means ± SD of three mice.

single infection, respectively (Fig. 5*C*). The $B220^{int}CD11c^+$ cell population in those four groups of mice decreased on day 9 postinfection (Fig. 5*A*, *lower panels*). Although $B220^{int}CD11c^+$ cells in *Pb* NK65-infected mice also expanded on day 6 postinfection, they were much less than those in coinfected or nonlethal parasite-infected mice. The cell population in *Pb* NK65-infected mice further expanded on day 9 postinfection, when no other groups of mice showed the expansion (Fig. 5*A*). The $B220^{int}CD11c^+$ cell population of spleen showed a similar pattern to that of peripheral blood (Fig. 5*B*), but the proportion of the cells in *Pb* NK65/*Pb* XAT-infected mice was lower than that in *Pb* XAT-infected mice on day 6 postinfection (Fig. 5*D*). These results suggested that coinfection with nonlethal parasites accelerated much more $B220^{int}CD11c^+$ cell expansion than did *Pb* NK65 single infection during the early phase of infection.

Coinfection with nonlethal parasites induces $CD4^+$ T cell expansion in spleen

We analyzed the kinetics of $CD4^+$ T cell expansion in spleen during single and mixed infection (Fig. 6). Significant expansion of splenic $CD4^+$ T cells in *Pb* XAT- or *Py* 17X-infected mice was observed from day 9 postinfection. In contrast, *Pb* NK65-infected mice did not show the increased levels of $CD4^+$ T cells even on day 9 postinfection. Mice coinfected with *Pb* NK65/*Pb* XAT or *Pb* NK65/*Py* 17X had almost the same number of splenic $CD4^+$ T cells as did *Pb* XAT- or *Py* 17X-infected mice, respectively.

Enhanced levels of IL-10 mRNA during coinfection and nonlethal infection

IFN-γ and IL-10 have been shown to be associated with protection and exacerbation during *P. berghei* and *P. yoelii* malaria (17, 18).

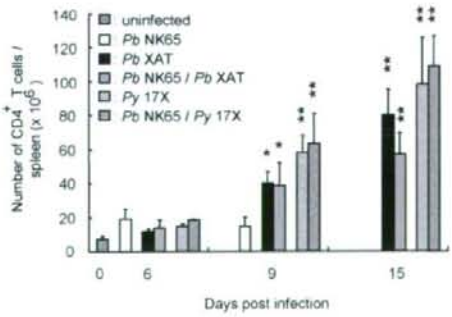

FIGURE 6. Coinfection with nonlethal parasites induces $CD4^+$ T cell expansion in spleen. Spleens were obtained from infected mice as described in the legend to Fig. 2 on days 6, 9, and 15 after infection and from uninfected mice. Splenic $CD3^+CD4^+$ cells were analyzed by flow cytometry and total numbers of $CD4^+$ T cells in spleen were calculated. Asterisks indicate a statistically significant difference (*, $p < 0.05$; **, $p < 0.005$ as compared with uninfected control mice). Results are expressed as means ± SD of three mice. Experiments were performed three times with similar results.

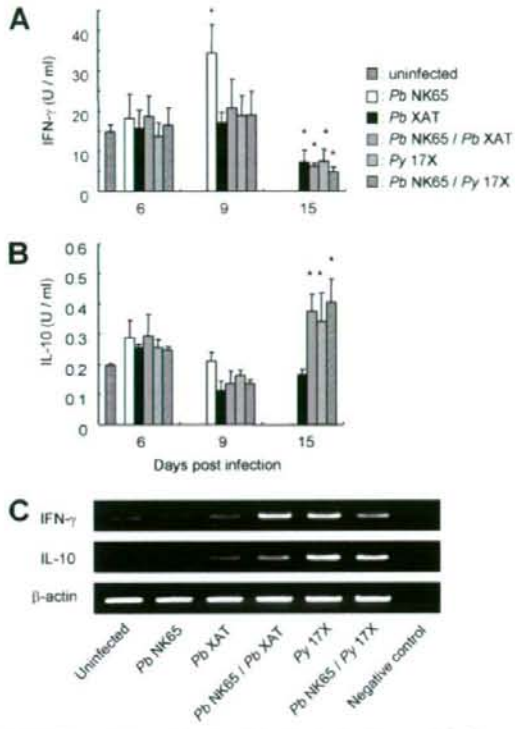

FIGURE 7. Enhanced levels of IL-10 mRNA during coinfection and nonlethal infection. *A* and *B*, Levels of IFN-γ or IL-10 were determined by ELISA. Plasma was collected from uninfected mice and infected mice on days 6, 9, and 15 post infection. *A*, Levels of IFN-γ in plasma. *B*, Levels of IL-10 in plasma. Asterisks indicate a statistically significant difference as compared with uninfected mice ($p < 0.001$). *C*, Total RNA was isolated from spleen of uninfected and infected mice as described in the legend to Fig. 2 on day 9 and subjected to RT-PCR using cytokine-specific primers. The samples without RNA template were used as negative control. Note that coinfected mice (*Pb* NK65/*Pb* XAT, *Pb* NK65/*Py* 17X) show IL-10 mRNA expression that is comparable to nonlethal parasite-infected mice (*Pb* XAT, *Py* 17X). Experiments were performed three times with similar results.

To examine whether these cytokines are associated with the suppression of *Pb* NK65-caused pathogenesis by coinfection with the nonlethal malaria parasites, we determined the levels of cytokines in plasma and cytokine mRNA in spleens from singly infected or coinfected mice (Fig. 7). *Pb* NK65 singly infected mice showed a high level of IFN-γ in plasma on day 9 compared with that in uninfected mice (Fig. 7*A*). Although the plasma IFN-γ levels in coinfected mice or nonlethal singly infected mice on days 6 and 9 were not different from those in uninfected mice, these mice showed significantly lower levels of IFN-γ than did uninfected mice on day 15. In contrast, strong IFN-γ mRNA expression was detected in the spleen from mice singly infected with *Py* 17X and coinfected with *Pb* NK65/*Pb* XAT and *Pb* NK65/*Py* 17X, compared with that observed in uninfected mice on day 9 (Fig. 7*C*). However, *Pb* NK65 singly infected mice did not show high levels of IFN-γ mRNA expression. These results suggested that spleen might not be a main organ for production of IFN-γ, which was involved in severe pathogenesis during *Pb* NK65 single infection (18), but the association of IFN-γ with suppressive pathogenesis by coinfection was still unclear.

The levels of IL-10 in plasma from single or coinfected mice on days 6 and 9 were not different from uninfected mice, but coinfected mice as well as nonlethal *Py* 17X singly infected mice showed elevated levels of IL-10 on day 15 (Fig. 7*B*). Although *Pb* NK65 singly infected mice showed only faint expression of IL-10 mRNA on day 9, mice coinfected with *Pb* NK65/*Pb* XAT or *Pb* NK65/*Py* 17X showed strong IL-10 mRNA expression, which was comparable to that observed in mice during *Pb* XAT or *Py* 17X single infection (Fig. 7*C*). IL-10 mRNA was not detected in spleen from uninfected mice. These results led us to hypothesize that the enhanced levels of IL-10 may be involved in suppression of pathogenesis during coinfection.

IL-10-deficient mice fail to receive benefits by coinfection with nonlethal malaria parasites

To examine whether IL-10 is associated with the suppression of the pathogenesis caused by coinfection, we determined the parasitemia, mortality, and the body weight of *Pb* NK65-infected IL-$10^{-/-}$ mice coinfected with *Pb* XAT or *Py* 17X. *Pb* NK65/*Pb* XAT-coinfected wild-type mice survived by day 21 (Fig. 8*D*), confirming the data obtained in Fig. 2*B*. In contrast, IL-$10^{-/-}$ mice coinfected with *Pb* NK65/*Pb* XAT began to die from day 10, and all mice died by day 21 postinfection (Fig. 8*D*) ($p = 0.034$). Moreover, their body weights were significantly lower than coinfected wild-type mice (Fig. 8*E*) ($p < 0.001$ on days 9, 11, and 13), although their parasitemia did not increase from day 11 (Fig. 8*F*). Similarly, *Pb* NK65/*Py* 17X-coinfected IL-$10^{-/-}$ mice began to die earlier than did wild-type mice (Fig. 8*G*), and their body weights were also lower than those of wild-type mice (Fig. 8*H*) ($p < 0.001$ on days 9, 13, and 18). During the period when coinfected IL-$10^{-/-}$ mice began to die, they developed liver injury (Fig. 8, *M* and *O*), which was not observed in coinfected wild-type mice (Fig. 8, *L* and *N*). In contrast, the parasitemia, mortality, the body weight, and development of liver injury of *Pb* NK65 singly infected IL-$10^{-/-}$ mice were not different from those of wild-type mice (Fig. 8, *A-C*, *J*, and *K*). Altogether, these results suggest that IL-10 may be involved in the suppressive effect of coinfection with nonlethal malaria parasites on the outcome of lethal *Pb* NK65 infection.

Discussion

In the present study, we investigated the influence of simultaneous infection with nonlethal murine malaria parasites, *Pb* XAT or *Py* 17X, on the outcome of the lethal *Pb* NK65 infection. *Pb* NK65 infection caused acute high parasitemia and pathogenesis, including body weight loss, severe anemia, and liver injury in mice. We found herein that the coinfection with nonlethal *Pb* XAT or *Py* 17X reduced such pathogenesis caused by *Pb* NK65 infection and prolonged survival of mice (Figs. 2–4). Because low levels of parasitemia and body weight loss in coinfected mice were observed from day 6 to 7 (Fig. 2), we postulated that T/B cell-mediated immunity would be involved in the suppressive effects of simultaneous infection with nonlethal parasites on lethal *Pb* NK65 infection and examined the response of dendritic cells and $CD4^+$ T cells.

The large expansion of $B220^{int}CD11c^+$ cells was observed in spleen and peripheral blood from coinfected mice on day 6, which was comparable to that from nonlethal parasite-infected mice (Fig. 5). These results suggest that expansion of $B220^{int}CD11c^+$ cells in coinfected mice may be accelerated by nonlethal parasite relative to lethal parasite infection. It has been reported that $CD11c^+$ dendritic cells are one of the professional APCs. As the murine plasmacytoid dendritic cell subset has been shown to coexpress CD11c and B220 (19–20), one would speculate that $B220^{int}CD11c^+$ cells expanded during nonlethal infection or coinfection might be one of the murine plasmacytoid dendritic cell subpopulations. Further characterization of the $B220^{int}CD11c^+$ cells, however, is needed for identification of these cells. In *Pb* NK65-infected mice, the peak expansion of $B220^{int}CD11c^+$ cells was observed on day 9, when these cells

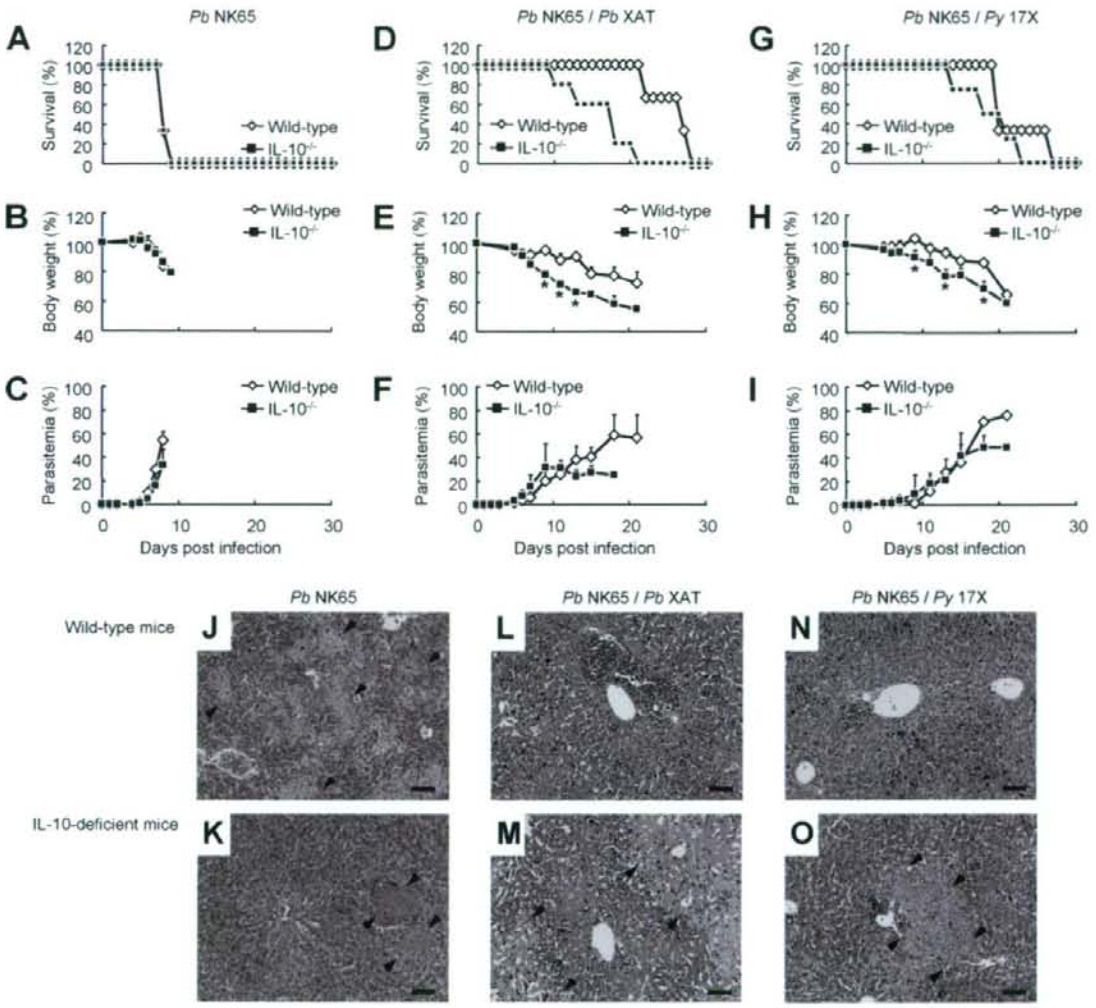

FIGURE 8. IL-10-deficient mice fail to receive benefits by coinfection with nonlethal malaria parasites. IL-$10^{-/-}$ mice and age-matched wild-type mice were singly infected with *Pb* NK65, coinfected with *Pb* NK65/*Pb* XAT, or coinfected with *Pb* NK65/*Py* 17X. Survival rates (*A*, *D*, and *G*), body weight (*B*, *E* and *H*), and course of parasitemia (*C*, *F*, and *I*) are shown. Asterisks indicate a statistically significant difference (*, $p < 0.001$ as compared with wild-type mice). Results are expressed as means ± SD of three to five mice. Histological analysis of liver was performed after staining with H&E (*J–O*). Livers were obtained from infected wild-type mice (*J*, *L*, and *N*) and IL-$10^{-/-}$ mice (*K*, *M*, and *O*) immediately after death from day 10 to 22 after infection. The scale bar indicates 100 μm. Arrowheads indicate focal necrosis of the liver cells. Experiments were performed twice with similar results and the representative data are shown.

began to decrease in coinfected mice as well as nonlethal *Pb* XAT- or *Py* 17X-infected mice. Because *Pb* NK65 parasites multiply quickly, especially in early phase of infection, earlier expansion of $B220^{int}CD11c^{+}$ cells may be the key for the suppression of pathogenesis during coinfection.

In contrast, mice coinfected with *Pb* NK65 and nonlethal *Pb* XAT or *Py* 17X showed increased levels of $CD4^{+}$ T cells from day 9 that were comparable to nonlethal parasite-infected mice (Fig. 6). Dendritic cells have been shown to activate naive T cells and play a crucial role in the initiation of immune responses (21–23). It is possible that the expansion of splenic $CD4^{+}$ T cells might be induced by $B220^{int}CD11c^{+}$ cells that had been expanded earlier (on day 6), and then the expanded $CD4^{+}$ T cells might be involved in suppression of pathogenesis in coinfected mice. $CD4^{+}$ T cells have been shown to play both protective and pathological roles during malaria infection (24–25). However, it seems that $CD4^{+}$ T cells would play protective roles during coinfection with lethal and nonlethal malaria parasites.

IL-10, which is produced by Th2 cells in $CD4^{+}$ T cell categories, inhibits inflammatory cytokines such as IFN-γ, TNF-α (26), and IL-12 (27). In malaria, IL-10 as well as TGF-β has been shown to be critical for host survival during *P. berghei* ANKA (28, 29) and *P. chabaudi* AS (30) infection. In the present study, *Pb* NK65/*Pb* XAT- or *Pb* NK65/*Py* 17X-coinfected mice showed high levels of IL-10 mRNA comparable to those in nonlethal *Pb* XAT- or *Py* 17X-infected mice (Fig. 7*C*), although *Pb* NK65-infected mice showed only a faint level of IL-10 mRNA. Moreover, high levels of IL-10 in plasma were followed by the IL-10 mRNA expression in coinfected mice on day 15 when IFN-γ production was

suppressed (Fig. 7). These results suggest that IL-10 may be involved in the suppression of pathogenesis in coinfected mice.

As expected, the suppressive effect of coinfection with nonlethal *Pb* XAT or *Py* 17X on severe body weight loss, liver injury, and mortality during *Pb* NK65 infection was reduced in IL-$10^{-/-}$ mice (Fig. 8), suggesting that IL-10 was involved in suppression of exacerbation of infection in simultaneous infection. The excessive inflammation has been shown to be able to account for body weight loss, liver injury, and mortality in mice infected with *Pb* NK65 (18, 31). Therefore, it is probable that enhancement of IL-10 would have suppressed the excessive inflammation caused by *Pb* NK65 and subsequently led to suppression of pathogenesis. In contrast, mortality as well as body weight loss in IL-$10^{-/-}$ mice during coinfection were not identical with those in *Pb* NK65 singly infected IL-$10^{-/-}$mice, suggesting that other regulatory factors, such as TGF-β (30), may be involved in suppression of pathogenesis.

In the late phase of infection, IL-$10^{-/-}$ mice coinfected with *Pb* NK65/*Pb* XAT or *Pb* NK65/*Py* 17X had lower levels of parasitemia than that in wild-type mice. These results suggest that although IL-10 plays an important role for suppression of liver injury, it may be also involved in suppression of clearance of malaria parasites and cause death by severe anemia in the late phase of coinfection. It has been shown that during *Py* 17XL lethal infection, IL-10 is involved in the exacerbation of infection because depletion of IL-10 prolonged survival of hosts and made some mice resolve the infection (17, 32, 33). IL-10 might have dual roles, protective and pathological, in mice coinfected with lethal and nonlethal malaria parasites.

Our findings showing the beneficial influence of coinfection with nonlethal *Pb* XAT or *Py* 17X to hosts during *Pb* NK65 infection indicate that suppression of disease severity induced by coinfection occurs in not only cerebral malaria but also pathogenesis such as body weight loss and liver injury. Our data suggest that the beneficial influence of coinfection with nonlethal malaria parasites may not be species-specific because a different species of malaria parasites, *Py* 17X, also induced protective immunity to *Pb* NK65 lethal infection by simultaneous infection (Fig. 2). In endemic areas, coinfections have made diagnosis and treatment difficult because host immune responses induced by each of the different *Plasmodium* spp. are mutually interfered with in a complicated manner. Results obtained from in vivo models of coinfection with murine malaria parasites would contribute to understand the host immune responses during mixed infection with different *Plasmodium* spp.

Disclosures

The authors have no financial conflicts of interest.

References

1. Snow, R. W., M. H. Craig, U. Deichmann, and D. le Sueur. 1999. A preliminary continental risk map for malaria mortality among African children. *Parasitol. Today* 15: 99–104.
2. Breman, J. G. 2001. The ears of the hippopotamus: manifestations, determinants, and estimates of the malaria burden. *Am. J. Trop. Med. Hyg.* 64: 1–11.
3. Siribal, S., S. Nakasiri, S. Looareesuwan, and P. Chavalitshewinkoon-Petmitr. 2004. Identification of human malaria parasites and detection of mixed infection in Thai patients by nested PCR. *Southeast Asian J. Trop. Med. Public Health* 35: 5–9.
4. Imwong, M., S. Pukrittayakamee, A. C. Grüner, L. Rénia, F. Letourneur, S. Looareesuwan, N. J. White, and G. Snounou. 2005. Practical PCR genotyping protocols for *Plasmodium vivax* using *Pvcs* and *Pvmsp1*. *Malar. J.* 4: 20.
5. Mehlotra, R. K., K. Lorry, W. Kastens, S. M. Miller, M. P. Alpers, M. Bockarie, J. W. Kazura, and P. A. Zimmerman. 2000. Random distribution of mixed species malaria infections in Papua New Guinea. *Am. J. Trop. Med. Hyg.* 62: 225–231.
6. Pinto, J., C. A. Sousa, V. Gil, L. Gonçalves, D. Lopes, V. E. do Rosário, and J. D. Charlwood. 2000. Mixed-species malaria infections in the human population of São Tomé island, west Africa. *Trans. R. Soc. Trop. Med. Hyg.* 94: 256–257.
7. Ebrahimzadeh, A., B. Fouladi, and A. Fazaeli. 2007. High rate of detection of mixed infections of *Plasmodium vivax* and *Plasmodium falciparum* in south-east of Iran, using nested PCR. *Parasitol. Int.* 56: 61–64.
8. Mason, D. P., F. E. McKenzie, and W. H. Bossert. 1999. The blood-stage dynamics of mixed *Plasmodium malariae-Plasmodium falciparum* infections. *J. Theor. Biol.* 198: 549–566.
9. Mason, D. P., and F. E. McKenzie. 1999. Blood-stage dynamics and clinical implications of mixed *Plasmodium vivax-Plasmodium falciparum* infections. *Am. J. Trop. Med. Hyg.* 61: 367–374.
10. McQueen, P. G., and F. E. McKenzie. 2006. Competition for red blood cells can enhance *Plasmodium vivax* parasitemia in mixed-species malaria infections. *Am. J. Trop. Med. Hyg.* 75: 112–125.
11. Luxemburger, C., F. Ricci, F. Nosten, D. Raimond, S. Bathet, and N. J. White. 1997. The epidemiology of severe malaria in an area of low transmission in Thailand. *Trans. R. Soc. Trop. Med. Hyg.* 91: 256–262.
12. Snounou, G., T. Bourne, W. Jarra, S. Viriyakosol, J. C. Wood, and K. N. Brown. 1992. Assessment of parasite population dynamics in mixed infections of rodent plasmodia. *Parasitology* 105: 363–374.
13. Voza, T., A. M. Vigario, E. Belnoue, A. C. Gruner, J. C. Deschemin, M. Kayibanda, F. Delmas, C. J. Janse, B. Franke-Fayard, A. P. Waters, et al. 2005. Species-specific inhibition of cerebral malaria in mice coinfected with *Plasmodium* spp. *Infect. Immun.* 73: 4777–4786.
14. Mitchell, A. J., A. M. Hansen, L. Hee, H. J. Ball, S. M. Potter, J. C. Walker, and N. H. Hunt. 2005. Early cytokine production is associated with protection from murine cerebral malaria. *Infect. Immun.* 73: 5645–5653.
15. Waki, S., J. Tamura, M. Imanaka, S. Ishikawa, and M. Suzuki. 1982. *Plasmodium berghei*: isolation and maintenance of an irradiation attenuated strain in the nude mouse. *Exp. Parasitol.* 53: 335–340.
16. Kobayashi, F., M. Niikura, S. Waki, T. Matsui, T. Fujino, T. Tsuruhara, and S. Kamiya. 2007. *Plasmodium berghei* XAT: contribution of γδ T cells to host defense against infection with blood-stage nonlethal malaria parasite. *Exp. Parasitol.* 117: 368–375.
17. Kobayashi, F., T. Morii, T. Matsui, T. Fujino, Y. Watanabe, W. P. Weidanz, and M. Tsuji. 1996. Production of IL-10 during malaria caused by lethal and nonlethal variants of *Plasmodium yoelii yoelii*. *Parasitol. Res.* 82: 385–391.
18. Waki, S., S. Uehara, K. Kanbe, K. Ono, M. Suzuki, and H. Nariuchi. 1992. The role of T cells in pathogenesis and protective immunity to murine malaria. *Immunology* 75: 646–651.
19. Nakano, H., M. Yanagita, and M. D. Gunn. 2001. $CD11c^+B220^+Gr\text{-}1^+$cells in mouse lymph nodes and spleen display characteristics of plasmacytoid dendritic cells. *J. Exp. Med.* 194: 1171–1178.
20. Bjorck, P. 2001. Isolation and characterization of plasmacytoid dendritic cells from Flt3 ligand and granulocyte-macrophage colony-stimulating factor-treated mice. *Blood* 98: 3520–3526.
21. Inaba, K., and R. M. Steinman. 1984. Resting and sensitized T lymphocytes exhibit distinct stimulatory (antigen-presenting cell) requirements for growth and lymphokine release. *J. Exp. Med.* 160: 1717–1735.
22. Knight, S. C., and A. J. Stagg. 1993. Antigen-presenting cell types. *Curr. Opin. Immunol.* 5: 374–382.
23. Metlay, J. P., M. D. Witmer-Pack, R. Agger, M. T. Crowley, D. Lawless, and R. M. Steinman. 1990. The distinct leukocyte integrins of mouse spleen dendritic cells as identified with new hamster monoclonal antibodies. *J. Exp. Med.* 171: 1753–1771.
24. Yoneto, T., T. Yoshimoto, C. R. Wang, Y. Takahama, M. Tsuji, S. Waki, and H. Nariuchi. 1999. Gamma interferon production is critical for protective immunity to infection with blood-stage *Plasmodium berghei* XAT but neither NO production nor NK cell activation is critical. *Infect. Immun.* 67: 2349–2356.
25. Langhorne, J., S. J. Meding, K. Eichmann, and S. S. Cillard. 1989. The response of $CD4^+$ T cells to *Plasmodium chabaudi chabaudi*. *Immunol. Rev.* 112: 71–94.
26. Mosmann, T. R., and K. W. Moore. 1991. The role of IL-10 in crossregulation of TH1 and TH2 responses. *Immunol. Today* 12: A49–A53.
27. Xu, X., K. Sumita, C. Feng, X. Xiong, H. Shen, S. Maruyama, M. Kanoh, and Y. Asano. 2001. Down-regulation of IL-12 p40 gene in *Plasmodium berghei*-infected mice. *J. Immunol.* 167: 235–241.
28. Tan, R. S., A. U. Kara, C. Feng, Y. Asano, and R. Sinniah. 2000. Differential IL-10 expression in interferon regulatory factor-1 deficient mice during *Plasmodium berghei* blood-stage infection. *Parasite Immunol.* 22: 425–435.
29. Kossodo, S., C. Monso, P. Juillard, T. Velu, M. Goldman, and G. E. Grau. 1997. Interleukin-10 modulates susceptibility in experimental cerebral malaria. *Immunology* 91: 536–540.
30. Li, C., L. A. Sanni, F. Omer, E. Riley, and J. Langhorne. 2003. Pathology of *Plasmodium chabaudi chabaudi* infection and mortality in IL-10-deficient mice are ameliorated by anti-tumor necrosis factor α and exacerbated by anti-transforming growth factor β antibodies. *Infect. Immun.* 71: 4850–4856.
31. Yoshimoto, T., Y. Takahama, C. R. Wang, T. Yoneto, S. Waki, and H. Nariuchi. 1998. A pathogenic role of IL-12 in blood-stage murine malaria lethal strain *Plasmodium berghei* NK65 infection. *J. Immunol.* 160: 5500–5505.
32. Omer, F. M., J. B. de Souza, and E. M. Riley. 2003. Differential induction of TGF-β regulates proinflammatory cytokine production and determines the outcome of lethal and nonlethal *Plasmodium yoelii* infections. *J. Immunol.* 171: 5430–5436.
33. Kobayashi, F., H. Ishida, T. Matsui, and M. Tsuji. 2000. Effects of in vivo administration of anti-IL-10 or anti-IFN-γ monoclonal antibody on the host defense mechanism against *Plasmodium yoelii yoelii* infection. *J. Vet. Med. Sci.* 6: 583–587.

BIOCHEMISTRY
including biophysical chemistry & molecular biology

Article

Structures of *Trypanosoma cruzi* Dihydroorotate Dehydrogenase Complexed with Substrates and Products: Atomic Resolution Insights into Mechanisms of Dihydroorotate Oxidation and Fumarate Reduction

Daniel Ken Inaoka, Kimitoshi Sakamoto, Hironari Shimizu, Tomoo Shiba, Genji Kurisu, Takeshi Nara, Takashi Aoki, Kiyoshi Kita, and Shigeharu Harada

Biochemistry, **2008**, 47 (41), 10881-10891• DOI: 10.1021/bi800413r • Publication Date (Web): 23 September 2008

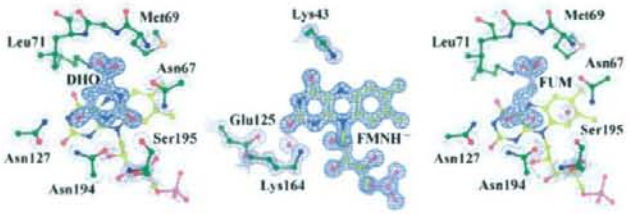

More About This Article

Additional resources and features associated with this article are available within the HTML version:

- Supporting Information
- Access to high resolution figures
- Links to articles and content related to this article
- Copyright permission to reproduce figures and/or text from this article

View the Full Text HTML